Water Purification Systems Using Cellulose-Based Nanofiber and Sponge Materials

著者（英）	ABDUL HALIM
内容記述	この博士論文は内容の要約のみの公開（または一部非公開）になっています
year	2019
その他のタイトル	セルロース系ナノファイバーとスポンジ材料を用いた水浄化システム
学位授与大学	筑波大学 (University of Tsukuba)
学位授与年度	2019
報告番号	12102甲第9279号
URL	http://hdl.handle.net/2241/00158017

Water Purification Systems Using Cellulose-Based Nanofiber and Sponge Materials

July 2019

ABDUL HALIM

Water Purification Systems Using Cellulose-Based Nanofiber and Sponge Materials

A Dissertation Submitted to
the Graduate School of Life and Environmental Sciences,
the University of Tsukuba
in Partial Fulfillment of the Requirements
for the Degree of Doctor of Philosophy in Bioresource Engineering
(Doctoral Program in Appropriate Technology and Sciences for Sustainable Development)

ABDUL HALIM

Table of Contents

Acknowledgments

In the name of Allah, the Beneficent, the Merciful. My Lord, increase me in knowledge. Praise be to Allah, the Cherisher and Sustainer of the Worlds.

I would like to express my sincere gratitude to my advisor, Prof. Toshiharu Enomae, who permit me to join his laboratory, support and encourage me during my PhD odessey. His style made my life in Japan so much enjoyfull. He is a teacher, colleague and father during my stay in Japan. I thanks to Prof. Mikio Kajiyama, Prof. Yasuhisa Adachi and Prof. Zhenya Zhang as my committee Thesis Advisor for their valuable advices.

I thank to Prof. Sugeng Winardi and Prof. Widiyastuti, my Bachelor and Master advisor, who encourage, inspired and recommended me to pursue a higher education. Their educate me patiently for my carelessness experiment. I thanks to Dr. Tantular Nurtono, Prof. Mukhtasor and Prof. Aries Sulistyono for his spiritual advices and motivational talk.

I sincerely thank to Mr. Mulyari (Alm), Mrs. Renita, Mr. Suja'i, Mr. Trimo, Mr. Aminah and all chemistry, physics, mathematics teachers of my senior high school who never given up on me. Their support mentally and financially during my high school have brough me to this far academic journey. I like to express my gratitude to Mr. Ach. Bahar (Alm), Mr. Dedi Effendi, Mrs. Eka, Mr. Supangat and all my elementary and junior high scholl teachers, who never tired to educate, motivate and push me to always has a big dream. I am very honor to has an inspiring teachers like them.

I thank to my mother, father, whole family for their support, sacrifice, hope and pray. Might Allah SWT rewards them the highest level of paradice. I thank to my wife for her love and meal during our life in Japan. To my dearest son, Ibrahim, who make me laugh and feel happy.

I am very thank to all lab members, Mrs. Shimazaki, Ms. Lin "Jane", Mr. Hu "Beibei", Mr. Yo, Mr. Kong, Mr. Nara, Ms. Takeuchi, Mr. Kitagawa, Mr. Fujino, Ms. Anting, Ms. Siti, Ms. Oyaizu, Mr. Morii, Ms. Zhang "Berry", Ms. Wang "Saya", Mr. Asayama, Dr. Xu "Chaoke", Dr. Evi, Dr. Srimonkon, Dr. Lee, and Dr. Mochizuki for their support make the laboratory environment very cheerfull.

I thank to Dr. Roni, Dr. Lilik, Dr. Nadia, Dr. Harsono, Dr. Kharistya Amaru, Dr. Haris, Mr. Karim, Mr. Akbar, Mr. Emha, Mr. Agil, Mr. Asep, Mr. Ridho, Ms. Nadia, Ms. Vanya, Mr. Guntur, Mr. Hadi, Mr. Eko, Mr. Yudhan, Mr. Haidar, Dr. Johny, Mr. Ali Fikry, Mr. Vicky, Mr. Teguh, FKMIT, PPI Ibaraki and all Indonesian people in Japan for their life support and help from my first live in Japan. I am sorry can not mention all of them even though your support is not the least.

The last, I am encourage all of my younger family and Indonesian people from Underrepresented/Disadvantaged background to educate your self and eager to pursue higher education.

Abbreviation and Symbol

ACC-CNF	Bomboo derived aqueous counter collision CNF
CI	Crystallinity index
CNF	Cellulose nanofiber
COD	Chemical oxygen demand
OCA	Oil contact angle
RR	Resilience ratio
TEMPO	2,2,6,6-tetramethylpiperidine-1-oxylradical
TOCNF	Wood-pulp based TEMPO-oxidized CNF
UP	Unrecoverable proportion
WCA	Water contact angle

θ	Contact angle Subscription A, R, S, W and CB refer to advancing, reciding, sliding, Wenzel and Cassie-Baxter, respectively Subscription S, L, V, O and W refer to solid, liquid, vapor, oil and water, respectively
I_a	Area under the amorphous peak.
I_t	Area under the crystalline peak
N_a	Concentration of water in the atmosphere
N_r	Concentration of water in the system
$P_{breakthrough}$	Breaktrough pressure
P_{ref}	Reference pressure
W_a	Compression work during the compression loading stages
W_b	Compression work during the compression unloading stages
k_c	Convective mass transfer coefficient
m_r	Mass remaining in the system
ε_a	Maximum strain
ε_b	Residual strain
$\Delta\theta_{\%}$	Hysteresis percentage
A	Robustness factor
d	Diameter of pore
f	Fraction of solid in contact with liquid
g	Gravitational acceleration
L	Contact length
Q	Volumetric flow rate
r	Roughness
γ	Surface tension
ΔP	Pressure drop
κ	Permeability
μ	Viscosity
ρ	Density
J	Mass transfer rate
t	Elapsed time

Abstract

Oily wastewater effluents have been increasing due to increased industrial activities and oil spill accidents. Conventional methods to separate an oil/water mixture are still laborious, release huge greenhouse effect gases, and occupy large processing space and long residence time. A sieving-based membrane shows a low separation efficiency, severe organic leakage, and high energy consumsion. The combination of sieving and hydrophobic/hydrophilic interaction on a superoleophobic fish mimicking surface was proposed to solve the conventional membrane disadvantages. Among other functional groups, a hydroxyl group has typical superoleophobic properties.

Cellulose is a biodegradable, sustainable and abundant material that used in many aspects of human life. Cellulose has been used in a wide range of filter application. Cellulose nanofibers refined by mechanically and chemically give different physical properties that determine the efficiency and efficacy of oil-water separation. In this research, surface properties and oil-water separation capabilities of two type of cellulose nanofibers (CNF): wood pulp-based 2,2,6,6-tetramethylpiperidine-1-oxylradical (TEMPO)-oxidized CNF (TOCNF) and bamboo-derived mechanical counter collision-processed CNF (ACC-CNF), were examinated. As supporting materials, cellulose sponge was fabricated through the xanthation method of dissolving cellulose followed by drying for regeneration.

To investigate surface properties of CNF in terms of oil contact angle under several concentrations of ethanol aqueous solution, Experimental and theoretically-estimated contact angles were compared. Those contact angles showed a large and small differences for high and low ethanol concentrations, respectively. The different surface properties included water absorbency, zeta potential, and surface roughness of a cellulose nanofiber layer under an aqueous environment. The TOCNF surface also had a surface like mucus fish scales. An antifouling experiment revealed that CNF were capable of repelling oil and exerting an antifouling effect.

For sponge fabrication, the drying process followed two steps: the first step was dominated by both convective mass and heat transfer due to mass and temperature differences between the sample and environment followed by the second step limited to a convective mass transfer after the sample temperature reaches that of the environment. When the Arrhenius equation was applied, the activation energy and pre-exponential factor during the convective mass transfer were -20.5 kJ K^{-1} mol^{-1} and 2250 m^{-2} s^{-1}, respectively. There was no tendency between the physical strength of obtained cellulose sponge and drying temperature. Addition of CNF to the xanthate did not affect the physical strength of the obtained cellulose sponge. However, the sponge obtained by drying at 65 ˚C showed more stable physical strength.

A cellulose sponge with CNF deposited was fabricated successfully. A cellulose sponge with relatively high physical strength acted as a supporting material, while CNF acted as an active, superoleophobic material. Deposition of TOCNF and ACC-CNF on inner pore surfaces of the sponge showed underwater superoleophobic and in-air oleophilic properties. A mucus-like layer of TOCNF enhanced oil repellency and provided separation efficiency greater than the ACC-CNF deposit. However, the mucus-like layer absorbed much water and decreased the flowrate. Oil-water separation testing demonstrated an excellent separation efficiency (>99%

and >98% for MCNF- and TCNF-membranes, respectively) and a high flowrate (3.73×10^3 and 166 L m^{-2} h^{-1} for MCNF- and TCNF membranes, respectively) with gravitational force alone.

Keywords: Oil water separation, superoleophobic, cellulose nanofiber

Chapter 1 Introduction

1.1 Background and Motivation

Water is an essential part of life. With the human population 7.5 billion in 2017 and predicted to be 8 billion in 2020, the fulfillment of water quality and quantity will become a big challenge (UN Population Division, 2017). Approximately 2 billion people live in an area of water scarcity and 1.6 billion people face an economical water shortage (FAO, 2007). Conversely, over 80% of wastewater is released to the environment without adequate treatment or reuse (WWAP, 2017). The fresh water is only 2.5% of total water on this earth, the water problems not solely related to domestic use but also to energy and food availability. Many energy production processes strongly need water to propel power plant turbines by steam or cool down the system. Meanwhile, water purification such as desalination consumes intensive of energy. Agriculture, livestock and animal ecosystem require unpolluted water as a habitat. However, since water has the capability to dissolve many things, water becomes easily contaminated with pollutants.

Economic growth in developing countries multiplies the industrial process and thus industrial wastewater. Oily wastewater is one of the effluents that are difficult to process since oil and water are both in liquid phases. Conventional wastewater treatment for liquid-liquid separation needs large space and long time. Palm oil wastewater needs 120 days only to reduce chemical oxygen demand (COD) from 50000 to 5000. Combining with a high plant capacity, a minimum volume of a lagoon to treat this wastewater is 40000 m^3 (Warstek, 2018). A conventional membrane for organic separation suffers from organic blockage and thus needs periodic cleaning. Ultrafiltration and nanofiltration membranes usually used for emulsion separation also consume intensive energy with a low separation efficiency. A polysulfone membrane with an average pore size of 3.62 nm (Chakrabarty, *et al*., 2010), modified polyvinylidene fluoride membrane with an average pore size of 6-8 nm (Yi *et al*., 2013), and ceramic membrane with an average pore size of 4 nm (Faibish & Cohen, 2001) exhibited an oil rejection and flux of 78.8% and 128 L m^{-2} h^{-1} bar^{-1}, 90% and 157 L m^{-2} h^{-1} bar^{-1}, and 95.5% and 201 L m^{-2} h^{-1} bar^{-1}, respectively.

Membrane separation is a divide on three fundamental principles: sieving, electrostatic phenomenon, and adsorption. Sieving membranes reject large particles ; molecular weight and molecular structure are an important parameter. Electrostatic membranes separate particles and water based on its charge so that the performanceis affected by charge and pH of the feed. Adsorption-based membranes are correlated with hydrophobic/hydrophilic interaction (wettability) between the membrane and particles so that the surface properties strongly matter

(Padaki, *et al*., 2015). Recent membrane researches combine the three principles to increase membrane efficacy.

In general, surface wettability is categorized to the affinity of the surface to the polar liquid such as water or non-polar liquid such as oil. Surfaces are classified into hydrophilic, hydrophobic and superhydrophobic types depending on the water contact angle (WCA): WCA $\leq 90°$, $90° < WCA < 150°$, and $WCA \geq 150°$, respectively. In line with the water contact angle, they are also classified into oleophilic, oleophobic or superoleophobic types depending on the oil contact angle (OCA): $OCA \leq 90°$, $90° < OCA < 150°$, and $OCA \geq 150°$, respectively. Since hydrophobic and superhydrophobic membranes usually encounter severe organic clogging and thus need periodic cleaning, oleophobic and superoleophobic membranes are proposed to overcome these problems (Huang & Wang, 2017). As the effect of hydrophobic surfaces are well-known and the related research was conducted for decades, superhydrophobic, oleophobic, and superoleophobic surfaces have recently attracted more attention. The number of studies regarding topics on oleophobicity increases by year as shown in Figure 1. Research on superhydrophobic surfaces increased more than that on oleophobic and superoleophobic surfaces. However, in the last five years, research on superoleophobic surfaces increased more significantly than that on oleophobic surfaces.

The wettability of membrane was controlled by modifying surface roughness, environment (in-air or underwater), and surface functional groups. The molecular dynamics simulation showed the underwater oleophobicity of several functional groups are, in order of increasing oleophobicity, methyl, amide, oligo ethylene-glycol, ethanolamine, hydroxyl, mixed-charged zwitterionic (Cheng, *et al*., 2017). Cellulose is a sustainable, abundant biomaterial that meet the criteria for the oleophobic membrane.

Cellulose has a hexagonal core in the chain and three hydroxyl group effective as a surface functional material for self-cleaning apparatus. Cellulose and its derivatives are widely used for filtration (Yuasa, *et al*., 1991; Ye, *et al*., 2002; Cho, *et al*., 2013; Tian *et al*, 2015; Chen, *et al*, 2018). Hydroxyl groups generated a result showing a high capability to repel oil and absorb water. Cellulose-derived products such as a TEMPO-oxidized cellulose nanofiber (CNF)-coated surface through layer-by-layer shows a better performance than poly(acrylic acid) (PAA) and poly(sodium, 4-styrene sulfonate) (PSS) (Huang & Wang, 2017). The PAA coated surfaces showed self-cleaning ability only in alkaline pH where acrylic acids were deprotonated. Meanwhile, CNF showed self-cleaning ability in both acidic and alkaline pH. However, this property was affected by ionic strength during depositing processes.

A general process to fabricate cellulose membrane is dissolution of cellulose followed by regeneration. Although cellulose has hydroxyl groups, cellulose has low dissolution to polar solvents such as water or ethanol. Cellulose also performs worse dissolution to the non-polar solvent. The principal reason is the strength of the internal bond between cellulose chains. The bond becomes stronger in the crystalline phase than the amorphous phase. The strong bond inhibits water molecules from penetrating and destroying the interaction. Another possible reason is that cellulose has amphiphilic properties (Lindman, *et al*., 2010; Medronho, *et al*., 2012; Mendronho & Lindman, 2015); hydrophilic site is hydroxyl group and hydrophobic site is glucopyranose ring. Therefore, the solvent must be capable to break both hydrophilic and hydrophobic bonds of cellulose.

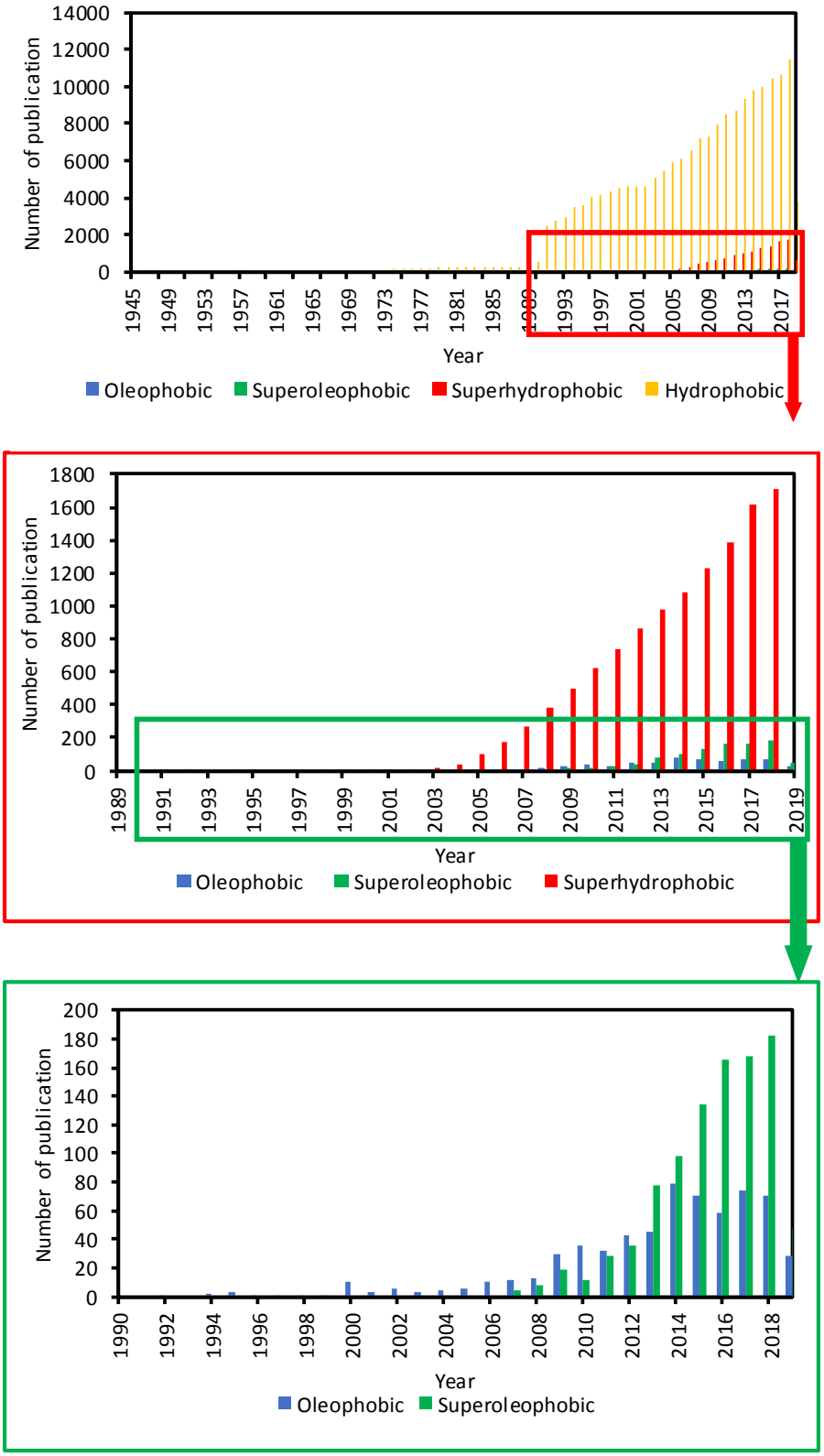

Figure 1.1 Number of publications published every year (Web of Science, accessed April 2019)

Cellulose is dissolved in several types of solvent. Scanning Electron Microscope (SEM) image of a regenerated cellulose dissolved in alkaline solvent has crystalline needle-like structure when dissolving in NaOH and become smoother when slightly non-polar additive such as urea or thiourea was added (Alves, *et al*., 2016a). However, the maximum solubility of cellulose in this NaOH/urea aqueous solution is below 4% (Wang, *et al*., 2016). In an acidic solvent, only smooth surface obtained and addition of surfactant to the cellulose solution generates a few pores due to foam generation (Alves, *et al*., 2016b). However, the acidic solvent significantly decreases the degree of polymerization of cellulose. The N-Methylmorpholine N-oxide (NMMO) solvent is able to dissolve cellulose up to around 30% (Peng, *et al*., 2017). Another known process is viscose method which cellulose first mercerized with high concentration NaOH followed by xanthation with CS_2, finally treated cellulose is dissolved in water. Dissolved cellulose can be easily treated for further purposes. To increase the performance of cellulose products, CNF is introduced. CNF with a high surface area to volume ratio is considered to increase the physical strength (Mittal, *et al*., 2018), surface wettability, and surface roughness (Rohrbach, *et al*., 2014).

1.2 Objective

This research aims to increase the knowledge of cellulose application for oily wastewater treatment. The mechanism of cellulose sponge fabrication was investigated. The surface characteristic of two types of CNF was performed and compared. The performance of a composite of cellulose nanofiber and cellulose sponge to separate oily wastewater was evaluated.

1.3 Outline of the Thesis

This thesis comprises six chapters. In chapter 1, the importance and motivation were explained. Chapter 2 describes the fundamental knowledge of surface and material engineering and its application to wastewater treatment. Chapter 3 will discuss the physical strength and surface properties of cellulose nanofiber sheets in-air and under an ethanol aqeous solution. Chapter 4 will discuss the fabrication of cellulose sponge and its potential as absorbent. The sponge was fabricated by xanthation followed by drying and the influence of temperature and drying time was discussed. The addition of cellulose nanofiber during fabrication was also examined. Chapter 5 will discuss the surface engineering of cellulose sponge and its application for oil-water separation. Chapter 6 is a general conclusion.

References

Alves, L., Medronho, B., Antunes, F. E., Topgaard, D., & Lindman, B. (2016a). Dissolution state of cellulose in aqueous systems. 1. alkaline solvents. *Cellulose*, 23, 247-258.

Alves, L., Medronho, B., Antunes, F. E., Topgaard, D., & Lindman, B. (2016b). Dissolution state of cellulose in aqueous systems. 2. acidic solvents. *Carbohydrate Polymers*, 151, 707-715.

Chakrabarty, B., Ghoshal, A. K., Purkait, M. K. (2010). Cross-flow ultrafiltration of stable oil-in-water emulsion using polysulfone membranes. *Chemical Engineering Journal*, 165(2), 447-456.

Chen, K., Xiao, C., Liu, H., Li, G., & Meng, X. (2018). Structure design on reinforced cellulose triacetate composite membrane for reverse osmosis desalination process. *Desalination*, 441, 35-43.

Cheng, G., Liao, M., Zhao, D., & Zhou, J. (2017). Molecular understanding on the underwater oleophobicity of self-assembled monolayers: zwitterionic versus nonionic. *Langmuir*, 33(7), 1732-1741.

Cho, D., Naydich, A., Frey, M. W., & Joo, Y. L. (2013). Further improvement of air filtration efficiency of cellulose filters coated with nanofibers via inclusion of electrostatically active nanoparticles. *Polymer*, 54(9), 2364-2372.

Faibish, R. S. & Cohen, Y. (2001). Fouling and rejection behavior of ceramic and polymer-modified ceramic membranes for ultrafiltration of oil-in-water emulsions and microemulsions. *Colloids and Surfaces A: Physicochemical and Engineering Aspects*, 191, 27-40

FAO. (2007). *Coping with water scarcity - Challenge of the twenty-first century.*

Huang, S., & Wang, D. (2017). A simple nanocellulose coating for self-cleaning upon water action: molecular design of stable surface hydrophilicity. A*ngewandte Chemie International Edition*, 56, 9053-9057.

Lindman, B., Karlstrom, G., & Stigsson, L. (2010). On the mechanism of dissolution of cellulose. *Journal of Molecular Liquids*, 156, 76-81.

Mittal, N., Ansari, F., Gowda.V, K., Brouzet, C., Chen, P., Larsson, P. T., Roth, S. V., Lundell, F., Wågberg, L., Kotov, N. A., and Söderberg, L. D. (2018). Multiscale control of nanocellulose assembly: transferring remarkable nanoscale fibril mechanics to macroscale fibers. *ACS Nano*, 12, 7, 6378-6388.

Medronho, B., Romano, A., Miguel, M. G., Stigsson, L., & Lindman, B. (2012). Rationalizing cellulose (in)solubility: reviewing basic physicochemical aspects and role of hydrophobic interactions. *Cellulose*, 19, 581-587.

Medronho, B., & Lindman, B. (2015). Brief overview on cellulose dissolution/regeneration interactions and mechanisms. *Advances in Colloid and Interface Science*, 222, 502-508.

Padaki, M., Murali, R. S., Abdullah, M. S., Misdan, N., Moslehyani, A., Kassim, M. A., Hilal, N., Ismail, A. F. (2015). Membrane technology enhancement in oil-water separation. A review. *Desalination*, 357, 197-207.

Peng, H., Dai, G., Wang, S., & Xu, H. (2017). The evolution behavior and dissolution mechanism of cellulose in aqueous solvent. *Journal of Molecular Liquids*, 241, 959-966.

Rohrbach, K., Li, Y., Zhu, H., Liu, Z., Dai, J., Andreasen, J., & Hu, L. (2014). A cellulose based hydrophilic, oleophobic hydrated filter for water/oil separation. *Chemical Communications*, 50, 13296-13299.

Tian, L., Zi-qiang, S., Jian-quan, W., & Mu-jia, G. (2015). Fabrication of hydroxyapatite nanoparticles decorated cellulose triacetate nanofibers for protein adsorption by coaxial electrospinning. *Chemical Engineering Journal*, 260, 818-825.

United Nations Population Division. (2017). *World Population Prospects 2017*. Retrieved August 22, 2017, from https://esa.un.org/unpd/wpp/DataQuery/

Wang, S., Lu, A., & Zhang, L. (2016). Recent advances in regenerated cellulose materials. *Progress in Polymer Science*, 53, 169-206.

Warstek (2018, Nov 5). TaW#4 Pengolahan limbah industri kelapa sawit. Speaker: Muhammad Ansori Nasution, Retrieved from https://youtu.be/6oPqbIzjySY

WWAP (United Nations World Water Assessment Programme). (2017). The united nations world water development report 2017. wastewater: the untapped resource. Paris: UNESCO.

Ye, S. H., Watanabe, J., Iwasaki, Y., & Ishihara, K. (2002). Novel cellulose acetate membrane blended with phospholipid polymer for hemocompatible filtration system. *Journal of Membrane Science*, 210(2), 411-421.

Yi, X. S., Yu, S. L., Shi, W. X., Wang, S., Sun, N., Jin, L. M., Ma, C. (2013). Estimation of fouling stages in separation of oil/water emulsion using nano-particles Al2O3/TiO2modified PVDF UF membranes. *Desalination*, 319, 38-46.

Yuasa, T., Ishikawa, G., Manabe, S.-i., Sekiguchi, S., Takeuchi, K., & Miyamura, T. (1991). The particle size of hepatitis c virus estimated by filtration through microporous regenerated cellulose fibre. *Journal of General Virology*, 72, 2021-2024.

Chapter 2 Literatures Review

2.1 Theory of Surface Wettability

2.1.1 Definition of Contact Angle

Wettability of a surface can be measured simply in terms of its contact angle (Fig. 2.1a) (θ) when some droplets of a liquid are put on the surface. However, it is still difficult to describe the wettability of the surface. Generously, wettability of the surface is measured by apparent contact angle. However, other parameters such as advancing and receding contact angles, contact angle hysteresis, sliding angle, and stickiness of liquid to the surface are also intoduced. The apparent contact angle is considered as the most thermodynamically stable contact angle. However, it is difficult to determine the thermodynamically stable condition in the experiment. Previously reported that the apparent contact angle is between advancing and receding contact angles (Andrieu, *et al.*, 1994). When a sessile drop volume is increased by adding a little more volume of the liquid, the boundary expands and the contact angle will increase. A maximum of contact angle before its boundary finishes expanding is termed the advancing contact angle (Fig. 2.1b) (θ_A). Conversely, the receding contact angle is defined as a minimum contact angle before its boundary shrinks due to a reduction of the drop volume (Fig. 2.1c) (θ_R). The differences between advancing and receding processes is defined as contact angle hysteresis.

The mobility of liquid also can be measured by sliding angle and stickiness. As shown in Figure 1d., when the solid surface is tilted, a droplet starts to slide. This minimum angle when the droplet begins to slide is defined as the sliding angle (θ_S) (Wang, *et al*., 2016). The surface wettability generously is classified according to the phobicity or philicity of the surface against fluid. Hydrophobic, oleophobic, and hemaphobic properties mean surfaces repelling water, oil, and blood, respectively and hydrophilic and oleophilic properties mean surfaces attracting water and oil, respectively. The term "icephobic" is also used to refer to the surface that prevents ice formation on it. Although the definitions of "superhydrophobic" and "superhydrophilic" are quite controversial, generally, the superhydrophobic surface can be defined as a surface with high water contact angle (>150°) and low contact angle hysteresis θ_S (<10°) . Otherwise, the superhydrophilic surface is defined as a surface with a low contact angle (5°) (Wang, *et al*., 2016). a liquid droplet can show a low contact angle and contact angle hysteresis so that the liquid easily slips on a solid surface (Fig. 2.1f) (Wang, *et al*., 2016). However, a liquid droplet can have both high contact angle and contact angle hysteresis θ_S so

that it still sticks to the surface even positioned vertically as is called the rose petal effect (Fig. 2.1g) (Feng, *et al*., 2008; Wang & Jiang, 2007; Jin, *et al*., 2005).

A contact angle reflects the affinity between liquid and a surface, while contact angle hysteresis reflects the mobility of liquid on the surface. However, it is still challenging to bring a quantitative value of contact angle hysteresis instead of a qualitative value. Hence, Korhonen *et al*. (2013) proposed the hysteresis percentage as defined as

$$\Delta\theta_{\%} = \frac{\cos\theta_R - \cos\theta_A}{2} \times 100\%, \tag{2.1}$$

where $\Delta\theta_{\%}$ is the hysteresis percentage ranging from 0% for no hysteresis to 100% for a maximum. The contact angle does not always change despite adding a little more volume to the droplet or pulling out from it, but shows almost constant advancing or receding contact angles.

When the volume of a droplet is increased by adding liquid, the contact angle will grow until some stable value while the contact line is subsequently growing (Fig. 2.2a). Similarly, for a receding contact angle, as a little volume of liquid is pulled out from the droplet, the contact angle decreases until some stable value and subsequently the contact line shrinks (Fig 2.2b). Only this stable condition provides the true advancing and receding contact angles. The amount of liquid added for measuring both advancing and receding contact angles can be calculated by solving the Young-Laplace equation or spherical cap model. The spherical cap model performs well only if the θ_A is lower than 120° or the hysteresis is small (for water). Otherwise, the Young-Laplace equation shows a good agreement between the model and experimental results. The spherical cap model is derived by considering a small droplet so that the gravitational force is neglected (The Bond number, $\Delta\rho g L^2/\gamma \ll 1$, where $\Delta\rho$, g, L and γ are the density difference between two phases, gravitational acceleration, contact length and surface tension, respectively). The spherical cap drop with contact angle θ has a volume as in Equation. (2.2).

$$\mathrm{V} = \frac{\pi}{3} R^3 [cos^3\theta - 3\cos\theta + 2]. \tag{2.2}$$

Substitions of advancing and receding contact angles θ_A and θ_R will provide V_A, V_R, R_A and R_R for advancing and receding volumes and radii, respectively as in Equation.(2.3).

$$\mathrm{V}_R = \left(\frac{(\cos^2\theta_R - 1)^2 (\cos\theta_R + 2)(1 - \cos^2\theta_R)^{-3/2}}{(\cos^2\theta_A - 1)^2 (\cos\theta_A + 2)(1 - \cos^2\theta_A)^{-3/2}} \right) \mathrm{V}_A \tag{2.3}$$

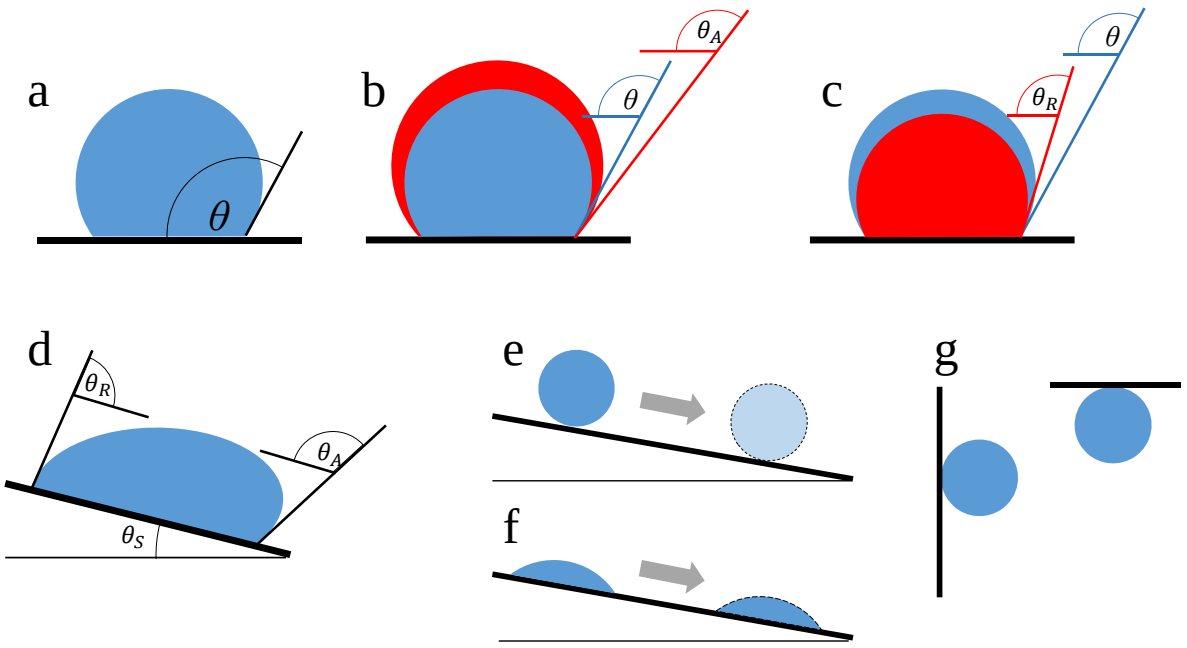

Figure 2.1 definition of contact angle (a), advancing contact angle (b), receding contact angle (c), sliding angle (d), super-repellent surface by high contact angle and low sliding angle (e), low contact angle but non-sticky (f) and high contact angle but sticky surface (g)

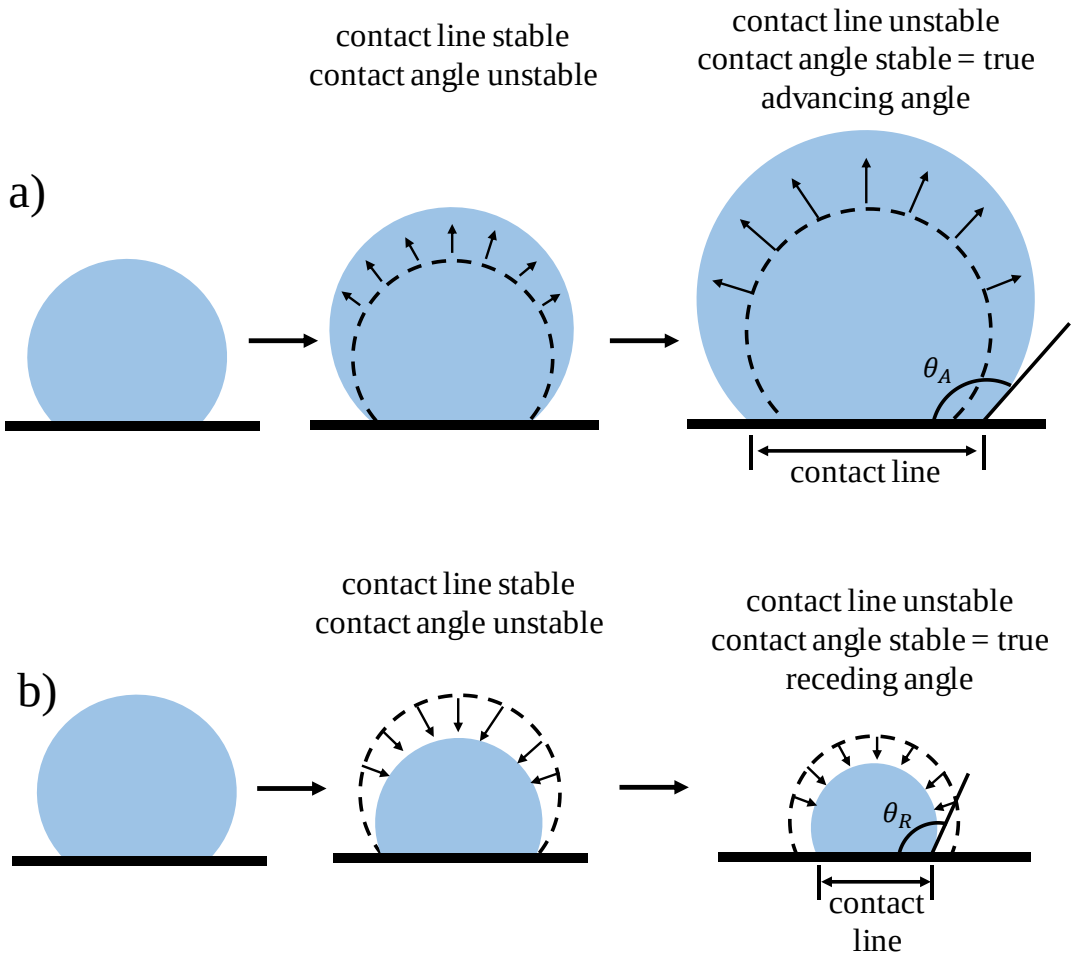

Figure 2.2. Illustration of true advancing (a) and receding (b) contact angle

2.1.2 Factor Determining Contact Angle

In 1805, Thomas Young published a paper about the correlation between surface tension and contact angle. Three forces employed on the line of contact angle that is interfacial tension of solid-liquid, solid-vapor, and liquid vapor. In the equilibrium, the sum of all forces is equal to zero (Fig. 2.3). In mathematical equation (Equation. 2.4 and 2.5) described as,

$$\gamma_{LV} \cos\theta + \gamma_{SL} - \gamma_{SV} = 0 \quad (2.4)$$

$$\cos\theta = \frac{\gamma_{SV} - \gamma_{SL}}{\gamma_{LV}}, \quad (2.5)$$

where, γ is the interfacial tension and subscripts S, L, and V refer to the solid, liquid and vapor phases, respectively. The equation is known as the Young equation (Young, 1805). Due to the surface tension of water that is higher than most oils, the contact angle of water are always higher than oils on smooth surfaces. Because the surface tension of liquid, fluid and solid is dependent on pressure, temperature, and impurities, the contact angle also depends on those variables.

a. Pressure

Pressure affects the interfacial interaction of two fluids because of a difference between the activities of them. A higher pressure of the fluid will increase the activity and decrease the interfacial tension at liquid-fluid and also solid-fluid interfaces (Li, *et al*., 2007). In further investigation, the contact angle is more dependent on activity than gas pressure. The pressure also influences contact angle hysteresis. The contact angle hysteresis of water on polystyrene surface under CO_2 environment is about 4-5° higher after depressurized than during being pressurize due to some CO_2 might be absorbed in the surface and remain during depressurize process make the surface more hydrophobic. Mathematical modeling confirms that gas might be absorbed to the solid surface.

b. Temperature

As surface tension is influenced by temperature, the contact angle is dependent on the liquid temperature. The surface tension of water is correlated linearly with the temperature (Claussen, 1967).

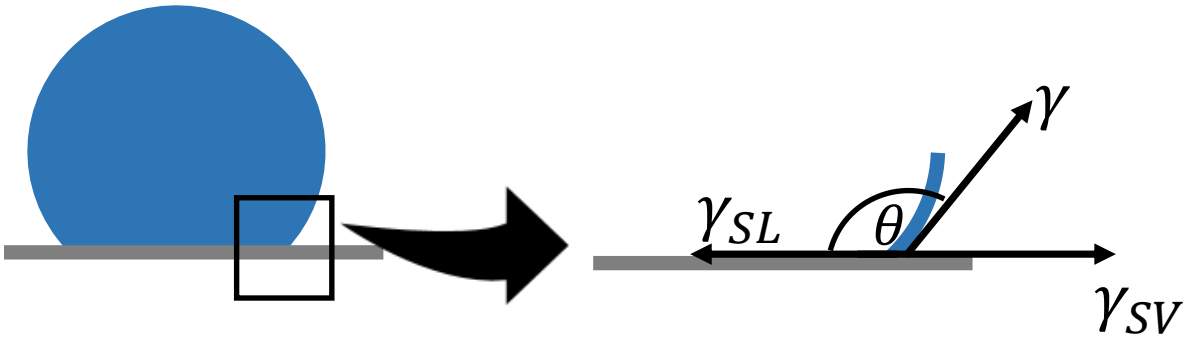

Figure 2.3 Illustration of force working in the droplet system

References

Ahmed, F. E., Lalia, B. S., Hilal, N., & Hashaikeh, R. (2014). Underwater Superoleophobic Cellulose/Electrospun PVDF-HFP Membranes for Efficient Oil/Water Separation. *Desalination*, 344, 48-54.

Amabili, M., Giacomello, A., Meloni, S., & Casciola, C. M. (2015). Unraveling the Salvinia Paradox: Design Principles for Submerged Superhydrophobicity. *Advanced Materials Interfaces*, 2, 1500248.

Barthlott, W., Schimmel, T., Wiersch, S., Koch, K., Brede, M., Barczewski, M., Walheim, S., Weis, A., Kaltenmaier, A., Leder, A., Bohn, H. F. (2010). The Salvinia Paradox: Superhydrophobic Surface with Hydrophilic Pins for Air Retention Under Water. *Advanced Materials*, 22, 2325-2328.

Bhushan, B., & Nosonovsky, M. (2010). The Rose Petal Effect and the Modes of Superhydrophobicity. *Philosophical Transactions of The Royal Society A*, 368, 4713-4728.

Bormashenko, E., Gendelman, O., & Whyman, G. (2012). Superhydrophobicity of Lotus Leaves versus Birds Wings: Different Physical Mechanisms Leading to Similar Phenomena. *Langmuir*, 28(42), 14992-14997.

Cassie, A. B., & Baxter, S. (1944). Wettability of Porous Surfaces. *Transactions of the Faraday Society*, 40, 546-551.

Chen, P.-C., & Xu, Z.-K. (2013). Mineral-Coated Polymer Membranes with Superhydrophylicity and Underwater Superoleophobicity for Effective Oil/Water Separation. *Scientific Reports*, 3, 2776.

Cheng, G., Liao, M., Zhao, D., & Zhou, J. (2017). Molecular Understanding on the Underwater Oleophobicity of Self-Assembled Monolayers: Zwitterionic versus Nonionic. *Langmuir*, 33(7), 1732-1741.

Cheng, Q., Ye, D., Chang, C., & Zhang, L. (2017). Facile Fabrication of Superhydrophilic Membranes Consisted of Fibrous Tunicate Cellulose Nanocrystals for Highly Efficient Oil/Water Separation. *Journal of Membrane Science*, 525, 1-8.

Claussen, W. F. (1967). Surface Tension and Surface Structure of Water. *Science*, 156, 1226-1227.

Ensikat, H. J., Ditsche-Kuru, P., Neinhuis, C., & Barthlott, W. (2011). Superhydrophobicity in Perfection: the Outstanding Properties of the Lotus Leaf. *Beilstein Journal of Nanotechnology*, 2, 152-161.

Fan, J.-B., Song, Y., Wang, S., Meng, J., Yang, G., Guo, X., Feng, L., Jiang, L. (2015). Directly Coating Hydrogel on Filter Paper for Effective Oil-Water Separation in Highly Acidic, Alkaline, and Salty Environment. *Advanced Functional Materials*, 25, 5368-5375.

Feng, L., Zhang, Y., Xi, J., Zhu, Y., Wang, N., Xia, F., & Jiang, L. (2008). Petal Effect: A Superhydrophobic State with High Adhesive Force. *Langmuir*, 24(8), 4114-4119.

Feng, X.-Q., Gao, X., Wu, Z., Jiang, L., & Zheng, Q.-S. (2007). Superior Water Repellency of Water Strider Legs with Hierarchical Structurer: Experiments and Analysis. *Langmuir*, 23(9), 4892-4896.

Gao, L., & McCarthy, T. J. (2007). How Wenzel and Cassie Were Wrong. *Langmuir*, 23(7), 3762-3765.

Gao, X., & Jiang, L. (2004). Water-repellent Legs of Water Striders. *Nature*, 432, 36.

Grigoryev, A., Tokarev, I., Kornev, K. G., Luzinov, I., & Minko, S. (2012). Superomniphobic Magnetic Microtextures with Remote Wetting Control. *Journal of the American Chemical Society*, 134(31), 12916-12919.

Huang, S., & Wang, D. (2017). A Simple Nanocellulose Coating for Self-Cleaning upon Water Action: Molecular Design of Stable Surface Hydrophilicity. *Angewandte Chemie International Edition*, 56, 9053-9057.

Jin, M., Feng, X., Feng, L., Sun, T., Zhai, J., Li, T., & Jiang, L. (2005). Superhydrophobic Aligned Polystyrene Nanotube Films with Adhesive Force. *Advanced Materials*, 17, 1977-1981.

Ju, G., Cheng, M., & Shi, F. (2014). A pH-Responsive Smart Surface for the Continuous Separation of Oil/Water/Oil Ternary Mixtures. *NPG Asia Materials*, 6, e111.

Kim, D. H., Jung, M. C., Cho, S.-H., Kim, S. H., Kim, H.-Y., Lee, H. J., Oh, K. H., Moon, M.-W. (2015). UV-Responsive Nano-Sponge for Oil Absorption and Desorption. *Scientific Reports*, 5, 12908.

Korhonen, J. T., Huhtamaki, T., Ikkala, O., & Ras, R. H. (2013). Reliable Measurement of the Receding Contact Angle. *Langmuir*, 29(12), 3858-3863.

Kota, A. K., Kwon, G., Choi, W., Mabry, J. M., & Tuteja, A. (2012). Hygro-responsive Membranes for Effective Oil-Water Separation. *Nature Communications*, 3, 1025.

Lafuma, A., & Quere, D. (2003). Superhydrophobic States. *Nature Materials*, 2, 457-460.

Li, Y., Pham, J. Q., Johnston, K. P., & Green, P. F. (2007). Contact Angle of Water on Polystyrene Thin Films: Effects of CO_2 Environment and Film Thickness. *Langmuir*, 23, 9785-9793.

Li, Y., Zhang, H., Fan, M., Zheng, P., Zhuang, J., & Chen, L. (2017). A Robust Salt-Tolerant Superoleophobic Alginate/Graphene Oxide Aerogel for Efficient Oil/Water Separation in Marine Environments. *Scientific Reports*, 7, 46379.

Liu, M., Wang, S., Wei, Z., Song, Y., & Jiang, L. (2009). Bioinspired Design of a Superoleophobic and Low Adhesive Water/Solid Interface. *Advanced Materials*, 21, 665-669.

Liu, J., Li, P., Chen, L., Feng, Y., He, W., & Lv, X. (2016). Modified Superhydrophilic and Underwater Superoleophobic PVDF Membrane with Ultralow Oil-Adhesion for Highly Efficient Oil/Water Emulsion Separation. *Materials Letters*, 185, 169-172.

Lu, F., Chen, Y., Liu, N., Cao, Y., Xu, L., Wei, Y., & Feng, L. (2014). A Fast and Convenient Cellulose Hydrogel-Coated Colander for High-Efficiency Oil-Water Separation. *RSC Advances*, 4, 32544-32548.

Movafaghi, S., Leszczak, V., Wang, W., Sorkin, J. A., Dasi, L. P., Popat, K. C., & Kota, A. K. (2017). Hemocompability of Superhemophobic Titania Surfaces. *Advanced Healthcare Materials*, 6(4), 1600717 (1-6).

Parker, A. R., & Lawrence, C. R. (2001). Water Capture by a Desert Beetle. *Nature*, 414, 33-34.

Peng, H., Wang, H., Wu, J., Meng, G., Wang, Y., Shi, Y., Liu, Z., Guo, X. (2016). Preparation of Superhydrophobic Magnetic Cellulose Sponge for Removing Oil from Water. *Industrial and Engineering Chemistry Research*, 55, 832-838.

Pi, P., Hou, K., Zhou, C., Wen, X., Xu, S., & Cheng, J. (2016). A Novel Superhydrophilic-Underwater Superoleophobic Cu2S Coated Copper Mesh for Efficient Oil-Water Separation. *Materials Letters*, 182, 68-71.

Rohrbach, K., Li, Y., Zhu, H., Liu, Z., Dai, J., Andreasen, J., & Hu, L. (2014). A cellulose Based Hydrophilic, Oleophobic Hydrated Filter for Water/Oil Separation. *Chemical Communication*, 50, 13296-13299.

Su, C., Yang, H., Song, S., Lu, B., & Chen, R. (2017). A Magnetic Superhydrophilic/Oleophobic Sponge for Continuous Oil-Water Separation. *Chemical Engineering Journal*, 309, 366-373.

Tian, D., Zhang, X., Tian, Y., Wu, Y., Wang, X., Zhai, J., & Jiang, L. (2012). Photo-Induced Water-Oil Separation Based on Switchable Superhydrophobicity-Superhydrophilicity and Underwater Superoleophobicity of the Aligned ZnO Nanorod Array-Coated Mesh Films. *Journal of Materials Chemistry*, 22, 19652-19657.

Tuteja, A., Choi, W., Ma, M., Mabry, J. M., Mazzella, S. A., Rutledge, G. C., McKinley, G. H., Cohen, R. E. (2007). Designing Superoleophobic Surfaces. *Science*, 318, 1618-1622.

Waghmare, P. R., Gunda, N. S., & Mitra, S. K. (2014). Under-water Superoleophobicity of Fish Scales. *Scientific Reports*, 4, 7454.

Wang, S., & Jiang, L. (2007). Definition of Superhydrophobic States. *Advanced Materials*, 19, 3423-3424.

Wang, S., Li, M., & Lu, Q. (2010). Filter paper with Selective Absorption and Separation of Liquids that Differ in Surface Tension. *ACS Applied Materials and Interfaces*, 2(3), 677-683.

Wang, Q., Yao, X., Liu, H., Quéré, D., & Jiang, L. (2015a). Self-removal of condensed water on the legs of water striders. *Proceeding of National Academy of Science*, 112(30), 9247-9252.

Wang, C.-F., Huang, H.-C., & Chen, L.-T. (2015b). Protonated Melamine Sponge for Effective Oil/Water Separation. *Scientific Reports*, 5, 14294.

Wang, G., He, Y., Wang, H., Zhang, L., Yu, Q., Peng, S., Wu, X., Ren, T., Zeng, Z., Xue, Q. (2015c). A Cellulose Sponge with Robust Superhydrophilicity and Under-water Superoleophobicity for Highly Effective Oil/Water Separation. *Green Chemistry*, 17, 3093-3099

Wang, G., Zeng, Z., Wang, H., Zhang, L., Sun, X., He, Y., Li, L., Wu, X., Ren, T., Xue, Q. (2015d). Low Drag Porous Ship with Superhydrophobic and Superoleophilic Surface for Oil Spills Cleanup. *ACS Applied Materials & Interfaces*, 7, 26184-26194.

Wang, Z., Elimelech, M., & Lin, S. (2016). Environmental Applications of Interfacial Materials with Special Wettability. *Environmental Science and Technology*, 50, 2132-2150.

Wang, C.-F., Yang, S.-Y., & Kuo, S.-W. (2017). Eco-Friendly Superwetting Material for Highly Effective Separations of Oil/Water Mixtures and Oil-in-Water Emulsions. *Scientific Reports*, 7, 43053.

Wenzel, R. N. (1936). Resistance of Solid Surfaces to Wetting by Water. *Industrial and Engineering Chemistry*, 28(8), 988-994.

Wenzel, R. N. (1949). Surface Roughness and Contact Angle. *Journal of Physical Chemistry*, 53(9), 1466-1467.

Xue, B., Gao, L., Hou, Y., Liu, Z., & Jiang, L. (2013). Temperature Controlled Water/Oil Wettability of a Surface Fabricated by a Block Copolymer: Application as a Dual Water/Oil On-Off Switch. *Advanced Materials*, 25, 273-277.

Xue, Z., Wang, S., Lin, L., Chen, L., Liu, M., Feng, L., & Jiang, L. (2011). A Novel Superhydrophilic and Underwater Superoleophobic Hydrogel-Coated Mesh for Oil/Water Separation. *Advanced Materials*, 23, 4270-4273.

Yang, J., Yin, L., Tang, H., Song, H., Gao, X., Liang, K., & Li, C. (2015). Polyelectrolyte-fluorosurfactant Complex-based Meshes with Superhydrophilicity and Superoleophobicity for Oil/Water Separation. *Chemical Engineering Journal*, 268, 245-250.

Ye, S., Cao, Q., Wang, Q., Wang, T., & Peng, Q. (2016). A Highly Efficient, Stable, Durable, and Recyclable Filter Fabricated by Femtosecond Laser Drilling of a Titanium Foil for Oil-Water Separation. *Scientific Reports*, 6, 37591.

Yin, K., Song, Y. X., Dong, X. R., Wang, C., & Duan, J. A. (2016). Underwater Superoleophobicity, Anti-Oil and Ultra-Broadband Enhanced Absorption of Metallic Surfaces Produced by a Femtosecond Laser Inspired by Fish and Chameleons. *Scientific Reports*, 6, 36557.

Yong, J., Chen, F., Yang, Q., Farooq, U., & Hou, X. (2015). Photoinduced Switchable Underwater Superoleophobicity-Superoleophilicity on Laser Modified Titanium Surfaces. *Journal of Materials Chemistry A*, 3, 10703-10709.

Young, T. (1805). An Essay on the Cohesion of Fluids. *Philosophical Transactions Royal Society Lond.*, 95, 65-87.

Yu, X., Wang, Z., Jiang, Y., Shi, F., & Zhang, X. (2005). Reversible pH-Responsive Surface: From Superhydrophobicity to Superhydrophilicity. *Advanced Materials*, 17, 1289-1293.

Zhang, L., Zhang, Z., & Wang, P. (2012). Smart Surfaces with Switchable Superoleophilicity and Superoleophobicity in Aqueous Media: Toward Controllable Oil/Water Separation. *NPG Asia Materials*, 4, e8.

Zhang, L., Zhong, Y., Cha, D., & Wang, P. (2013). A Self-Cleaning Underwater Superoleophobic Mesh for Oil-Water Separation. *Scientific Reports*, 3, 2326.

Zhang, W., Zhu, Y., Liu, X., Wang, D., Li, J., Jiang, L., & Jin, J. (2014). Salt-Induced Fabrication of Superhydrophilic and Underwater Superoleophobic PAA-g-PVDF Membranes for Effective Separation of Oil-in-Water Emulsions. *Angewandte Chemie International Edition*, 53, 856-860.

Zhou, K., Zhang, Q. G., Li, H. M., Guo, N. N., Zhu, A. M., & Liu, Q. L. (2014). Ultrathin Cellulose Nanosheet Membranes for Superfast Separation of Oil-in-Water Nanoemulsions. *Nanoscale*, 6, 10363-10369.

Chapter 3 Surface Properties of Cellulose Nanofiber and Its Application for Anti Fouling

3.1 Introduction

Antifouling properties of materials were applied to various purposes especially to membranes. Antifouling properties avoid the blockage caused by bacteria, oil and other organic matters. Two approaches were applied to production of antifouling materials. The first approach was superoleophobization that is marked by a high contact angle (>150°). The second approach was providing slipperiness, that is, making a liquid slip well on the surface inspired by *Nepenthes* pitcher plant (Wong, *et al*., 2011). The slipperiness approach did not need a high contact angle or the surface containing a non-soluble fluid that repels the targeted liquid.

The effort to fabricate a slippery surface from cellulose was reported by Guo, *et al*. (2014) and Chen, *et al*. (2014). Cellulose was modified with lauroyl chloride to generate cellulose lauroyl ester and perfluoropolyether was used as oil lubricant (Chen, *et al*., 2014). Hydrophobic and hydrophilic slippery surfaces were attempted to produce by reacting cellulose with vinyl groups and polar groups (cysteamine or 2-mercaptoethanol), respectively (Guo, *et al*., 2014). However, the high surface roughness and low solubility of cellulose in common solvents limited the application of cellulose as a slippery surface.

The cellulose nanofiber sheet with high surface rougness is a candidate as an antifouling material both by the hydrophilic slippery surface and underwater superoleophobic surface. In underwater condision, the contact angle was influenced by the interfacial tension of both fluids (targeted liquid and the environment). Derived from the general Young equation of contact angle under in-air condision, the equation of contact angle underwater expressed as (Liu, *et al*., 2009) Equation. (2.10).

$$\cos\theta_{OW} = \frac{\gamma_{OA}\cos\theta_{OA} - \gamma_{WA}\cos\theta_{WA}}{\gamma_{OW}}, \tag{2.10}$$

where γ and θ are the surface tension at the interface between the two phases and contact angle, respectively. Subscrpts S, A, W and O refer to the solid, air, water and oil, respectively. In this experiment, the surface properties of cellulose nanofiber was investigated under various levels of surface tension.

References

Arima, Y. & Iwata, H. (2007). Effect of wettability and surface functional groups on protein adsorption and cell adhesion using well-defined mixed self-assembled monolayers. *Biomaterials*, 28, 3074-3082

Chen, L., Geissler, A., Bonaccurso, E., Zhang, K. (2014). Transparent slippery surfaces made with sustainable porous cellulose lauroyl ester films. *ACS Applied Materials & Interfaces*, 6 (9), 6969-6976.

Guo, J., Fang, W., Welle, A., Feng, W., Filpponen, I., Rojas, O. J., and Levkin, P. A. (2014). Superhydrophobic and slippery lubricant-infused flexible transparent nanocellulose films by photoinduced thiol–ene functionalization. *ACS Applied Materials & Interfaces*, 8(49), 34115-34122.

Isogai, A., Saito, T., Fukuzumi, H.(2011). TEMPO-oxidized cellulose nanofibers. *Nanoscale*, 3, 71-85.

Lee, J. H., Khang, G., Lee, J. W., Lee, H. B. (1998). Interaction of different types of cells on polymer surfaces with wettability gradient. *Journal of colloid and interface science*, 205, 323-330.

Liu, M., Wang, S., Wei, Z., Song, Y., & Jiang, L. (2009). Bioinspired Design of a Superoleophobic and Low Adhesive Water/Solid Interface. *Advanced Materials*, 21, 665-669.

Roger, K., & Cabane, B. (2012). Why Are Hydrophobic/Water Interfaces Negatively Charged? *Angewandte Chemie, 124*, 5723-5726.

Vazques, G., Alvarez, E., Navaza, J. M. (1995). Surface tension of alcohol water + water from 20 to 50 °C. *Journal of Chemical & Engineering Data*, 40 (3), 611-614.

Waghmare, P. R., Gunda, N. S., & Mitra, S. K. (2014). Under-water Superoleophobicity of Fish Scales. *Scientific Reports*, 4, 7454.

Wohlfarth, C. (2016). *Surface tension of tetradecane*. In: Lechner M.D. (eds) Surface Tension of Pure Liquids and Binary Liquid Mixtures. Landolt-Börnstein - Group IV Physical Chemistry (Numerical Data and Functional Relationships in Science and Technology), vol 28. Springer, Berlin, Heidelberg.

Wong, T.-S., Kang, S. H., Tang, S. K. Y., Smythe, E. J., Hatton, B. D., Grinthal, A., Aizenberg, J. (2011). Bioinspired self-repairing slippery surfaces with pressure-stable omniphobicity. *Nature*, 477, 443–447.

Zhou, G., Xu, C., Cheng, W., Zhang, Q., Nie, W. (2015). Effects of Oxygen Element and Oxygen-Containing Functional Groups on Surface Wettability of Coal Dust with

Various Metamorphic Degrees Based on XPS Experiment. *Journal of Analytical Methods in Chemistry*, 2015, Article ID 467242

Chapter 4 Fabrication of Cellulose Sponge: Effect of drying temperature and cellulose nanofiber addition on the physical strength

4.1 Introduction

Cellulose is an attractive biomaterial because of its abundant-availability, sustainability, and zero carbon trace. Recently, cellulose sponge was developed for a more sophisticated purpose such as implant (Märtson, *et al*., 1999), three-dimensional cell culture scaffold, temperature responsive material (Du, *et al*., 2018), lithium battery electrode and wearable thermoelectric material (Cheng, *et al*., 2018). Freeze-drying, gas forming, and template method were generally used to produce cellulose sponge. For freeze-drying, cellulose or cellulose derivative suspension was pretreated or directly cooled at low temperature then dried at a vacuum condition. Regenerated cellulose (RC) from cellulose acetate (CA) was freeze-dried at -110 °C has a tensile strength of approximately 140 kPa and Young's modulus approximately 2.7 N mm^{-2} (Gustaite *et al*., 2015). Electrospinning was conducted as pre-treatment to produce fiber mat from the CA solution. Obtained CA mat then deacetylated to produce RC by sodium hydroxide solution in a water-ethanol solvent. RC then dilute in the solvent then dried by vacuum drying or freeze-drying (Xu, *et al*., 2018). Gas foaming by sodium borohydride was reported to produce a porous structure of RC mat (Joshi, *et al*., 2016). Sodium borohydride reacted with water and release hydrogen gas followed by vacuum drying (Joshi, *et al*., 2015).

The physical properties of cellulose such as compression stress, recoverable ability or stiffness are essential parameters. Three-dimensional structure of a material such as porosity and pore size significantly affect the physical properties. Freeze-drying and gas forming methods were more difficult to control the porosity and pore size of a cellulose sponge than the templating method. The templating method was used mainly in many porous productions (Wang, *et al*., 2017; Peng, *et al*., 2016; Nandiyanto & Okuyama, 2011). This method easily controlled either porosity or pore size by selecting the type and size of a template or process temperature. Additives were also used to improve physical strength. Cellulose nanofibers (CNF) as an additive was applied to improve water retention (Kose, *et al*., 2011) and physical strength of paper (Boufi, *et al*., 2016; Petroudy *et al*., 2017), or polymer composite (Lee, *et al*., 2018; Sakakibara, *et al*., 2017).

References

Boufi, S., González, I., Delgado-Aguilar, M., Tarrès, Q., Pèlach, M. À., & Mutjé, P. (2016). Nanofibrillated cellulose as an additive in papermaking process: A review. Carbohydrate Polymers, 154, 151-166.

Cheng, H., Du, Y., Wang, B., Mao, Z., Xu, H., Zhang, L., Zhong, Y., Jiang, W., Wang L., Sui, X. (2018). Flexible cellulose-based thermoelectric sponge towards wearable pressure sensor and energy harvesting. *Chemical Engineering Journal*, 338, 1-7.

Du, Y., Cheng, H., Li, Y., Wang, B., Mao, Z., Xu, H., Zhang, L., Zhong, Y., Yan, X., Sui, X. (2018). Temperature-responsive cellulose sponge with switchable pore size: Application as a water flow manipulator. *Materials Letters*, 210, 337-340.

Geankoplis, C. J. (1993). Transport processes and unit operations. Englewood Cliffs, New Jersey: Prentice Hall.

Gustaite, S., Kazlauske, J., Bobokalonov, J., Perni, S., Dutschk, V., Liesiene, J., & Prokopovich, P. (2015). Characterization of cellulose based sponges for wound dressings. Colloids and Surfaces A: Physicochemiscal and Engineering Aspects, 480, 336-342.

Isogai, A., Saito, T., & Fukuzumi, H. (2011). TEMPO-oxidized Cellulose Nanofibers. Nanoscale, 3, 71-85.

Jiang, F., Kondo, T., & Hsieh, Y.-L. (2016). Rice straw cellulose nanofibrils via aqueous counter collision and differential centrifugation and Their self-assembled structures. ACS Sustainable Chem. Eng., 4(3), 1697-1706.

Jin, M., Feng, X., Feng, L., Sun, T., Zhai, J., Li, T., & Jiang, L. (2005). Superhydrophobic Aligned Polystyrene Nanotube Films with Adhesive Force. Advanced Materials, 17, 1977-1981.

Joshi, M. K., Pant, H. R., Tiwari, A. P., Kim, H. J., Park, C. H., & Kim, C. S. (2015). Multi-layered macroporous three-dimensional nanofibrous scaffold via a novel gas foaming technique. *Chemical Engineering Journal*, 275, 79-88.

Joshi, M. K., Pant, H. R., Tiwari, A. P., Maharjan, B., Liao, N., Kim, H. J., Park, C. H., Kim, C. S. (2016). Three-dimensional cellulose sponge: Fabrication, characterization, biomimetic mineralization, and in vitro cell infiltration. *Carbohydrate Polymers*, 136, 154-162.

Jozala, A. F., de Lencastre-Novaes, L. C., Lopes, A. M., & Santos-Ebinuma, V. d. (2016). Bacterial nanocellulose production and application: a 10-year overview. *Applied Microbiology and Biotechnology*, 100(5), 2063-2072.

Kondo, T., Kose, R., Naito, H., & Kasai, W. (2014). Aqueous counter collision using paired water jets as a novel means of preparing bio-nanofibers. *Carbohydrate Polymers*, 112, 284-290.

Kose, R., Kasai, W., & Kondo, T. (2011). Switching surface properties of substrates by coating with a cellulose nanofiber having a high adsorbability. *Sen'i Gakkaishi*, 67(7), 163-167.

Kubo, J., Nakatsubo, T., Ito, K., Tajima, H. (2018, September 27). United State Patent No: US 2018 / 0273644 A1.

Lee, J.-C., Lee, J.-A., Lim, D.-Y., & Kim, K.-Y. (2018). Fabrication of cellulose nanofiber reinforced thermoplastic composites. *Fibers and Polymers*, 19(8), 1753-1759.

Lundahl, M. J., Cunha, A. G., Rojo, E., Papageorgiou, A. C., Rautkari, L., Arboleda, J. C., & Rojas, O. J. (2016). Strength and water interactions of cellulose I filaments wet-spun from cellulose nanofibril hydrogels. Scientific Reports, 6, Articles number 30695. doi:https://doi.org/10.1038/srep30695

Lyu, S., Yang, X., Shi, D., Qi, H., Jing, X., & Li, S. (2017). Effect of High Temperature on Compression Property and Deformation Recovery of Ceramic Fiber Reinforced Silica Aerogel Composites. Science China Technological Sciences, 60(11), 1681-1691.

Märtson, M., Märtson, M., Viljanto, J., Hurme, T., Laippala, P., & Saukko, P. (1999). Is cellulose sponge degradable or stable as implantation material? An in vivo subcutaneous study in the rat. Biomaterials, 20(21), 1989-1995. Retrieved 1 9, 2019, from https://sciencedirect.com/science/article/pii/s0142961299000940

Nandiyanto, A. B., & Okuyama, K. (2011). Progress in developing spray-drying methods for the production of controlled morphology particles: From the nanometer to submicrometer size ranges. *Advanced Powder Technology*, 22(1), 1-19.

Nam, S., French, A. D., Condon, B. D., & Concha, M. (2016). Segal crystallinity index revisited by the simulation of X-ray diffraction patterns of cotton cellulose Iβ and cellulose II. Carbohydrate Polymers, 135, 1-9.

Peng, H., Wang, H., Wu, J., Meng, G., Wang, Y., Shi, Y., Liu, Z., Guo, X. (2016). Preparation of Superhydrophobic Magnetic Cellulose Sponge for Removing Oil from Water. *Industrial and Engineering Chemistry Research*, 55, 832-838

Peng, H., Dai, G., Wang, S., & Xu, H. (2017). The Evolution Behavior and Dissolution Mechanism of Cellulose in Aqueous Solvent. Journal of Molecular Liquids, 241, 959-966.

Petroudy, S. R., Sheikhi, P., & Ghobadifar, P. (2017). Sugarcane bagasse paper reinforced by cellulose nanofiber (CNF) and bleached softwood kraft (BSWK) pulp. *Journal of Polymers and the Environment*, 25(2), 203-213.

Sakakibara, K., Moriki, Y., Yano, H., & Tsujii, Y. (2017). Strategy for the improvement of the mechanical properties of cellulose nanofiber-reinforced high-density polyethylene nanocomposites using diblock copolymer dispersants. ACS Applied Materials & Interfaces, 9(50), 44079-44087.

Wang, Y., Qian, J., Zhao, N., Liu, T., Xu, W., & Suo, A. (2017). Novel hydroxyethyl chitosan/cellulose scaffolds with bubble-like porous structure for bone tissue engineering. *Carbohydrate Polymers*, 167, 44-51.

Xu, T., Wang, Z., Ding, Y., Xu, W., Wu, W., Zhu, Z., & Fong, H. (2018). Ultralight electropspun cellulose sponge with super-high capacity on absorption of organic compounds. Carbohydrate Polymers, 179, 164-172.

Chapter 5 Fabrication of Cellulose Nanofiber-Deposited Cellulose Sponge as Oil-Water Separation Membrane

5.1 Introduction

Although oil and water are immiscible, water treatment for oily wastewater is still laborious. Oil leakage from petroleum or offshore drilling usually requires oil dispersants or oil boom techniques (Committee., 2013). Oil dispersants dissolve oil in seawater to reduce the oil amount at the water level. However, this increases the oil concentration of seawater and may contaminate the underwater organism ecology (Coelho, *et al*., 2013). Oil booms isolate an oil spill and allowing the oil to be absorbed using sponge materials (Song, *et al*., 2014). While palm oil mill effluent is generally treated in an open lagoon that required large space and long residence time, releasing huge quantities of greenhouse gas (Nasution, *et al.*, 2018). To address this issue, membrane technology was introduced (Padaki, *et al*., 2015). A life cycle assessment showed that a membrane required a minimum amount of energy among existing methods (Nasution, *et al.*, 2018) and wettability based membrane was effective for oil water separation (Wang, *et al*., 2016).

There are several methods of wettability modification, for example, hydrophobic, oleophobic, and Janus modification. The hydrophobic membrane is permeated by oil and rejects water; the oleophobic membrane is penetrated by water and rejects oil; Janus membrane is hydrophobic on one side and hydrophilic on the other side. The wettability of the membrane depends on the surface tension of oil and water and surface energy of the membrane (Wang, *et al*., 2016; Yang, *et al*., 2016).

Oleophilic membranes usually suffer from organic blockage and require periodic cleaning. To overcome these problems, oleophobic membranes were proposed to prevent organic blockage and exhibit a self-cleaning property (Huang & Wang, 2017). The wettability of the membrane surface was modified by introducing functional groups, increasing roughness, or combination of them (Tuteja, *et al*., 2007). Scaffold materials for membrane have a wide variety ranging from metal to synthetic and natural polymers. Stainless steel mesh coated with polyacrylamide hydrogel (Xue, *et al*., 2011), ZnO (Tian, *et al*., 2012), MnO_2 nanowires modified with multiwalled carbon nanotubes (Yue, *et al*., 2018) and polyelectrolyte-fluorosurfactant/SiO_2 (Yang, *et al*., 2015) was reported to provide superoleophobic and superhydrophilic properties. The increasing surface roughness of titanium foil (Ye, *et al.*, 2016) and copper mesh (Pi, *et al*., 2016) using femtosecond laser ablation and anodization,

respectively were also reported. Titanium (Ti) foil and copper (Cu) mesh both showed superoleophobicity and superhydrophilicity.

Synthetic polymers such as poly-acrylic acid-modified polyvinylidene fluoride membranes (Zhang, *et al.*, 2014), polysulfonate (Obaid, *et al.*, 2018), polyacrylonitrile (Zhang, *et al*., 2016), plasma-treated polycarbonate (Zeiger, *et al*., 2017), and melamine sponges (Su, *et al*., 2017; Wang, *et al.*, 2015a) were reported to have superhydrophilicity and exhibit good performance in oil-water separation. Natural polymers such as alginate (Li, *et al*., 2017), chitosan (Wang, *et al*., 2017a), guar-gum (Dai, *et al*., 2017), and cellulose-based membranes (Wang, *et al*., 2015b) have been applied. However, a natural polymer, especially cellulose-based membrane, had a low physical strength (Fan, *et al*., 2015; Rohrbach, *et al*., 2014), expensive fabrication process (Zhou, *et al*., 2014; Ao, *et al*., 2017), and thus requires modification with synthetic polymers (Wang, *et al*., 2017b). Nylon filter paper was also used as a supporting material modified with cellulose nanocrystals (Cheng, *et al*., 2017) or cellulose microcrystals (Chen, *et al*., 2014).

To the best of our knowledge, almost no research for creating superoleophobic or superhydrophilic membranes consisting of only natural polymers and modified with CNF have been reported. In this research, we investigated properties of a cellulose sponge fabricated through xanthation and heating, and then deposited ACC-CNF and TOCNF on the sponge surface. The possibility of a CNF-deposited cellulose sponge to improve the performance of oil-water separation was also evaluated.

5.2 Experimental

1.1 Cellulose sponge fabrication

The sponge fabrication was as same as explained in section 4.2 with minor modification. The drying condition was 65°C for 6 h. Solvent exchange was conducted to remove water from the membrane by soaking the membrane in ethanol (Wako Pure Chemical Industries Ltd., Japan) followed by acetone (Wako Pure Chemical Industries Ltd., Japan) for 2 and 3 days, respectively to prevent shrinkage. From this process, 0.1231 g of dried regenerated cellulose sponge was obtained.

1.2 CNF-deposited membrane fabrication

A 1.08% aqueous dispersion of TEMPO (2,2,6,6-tetramethylpiperidine-1-oxyl)-oxidized wood pulp-based cellulose nanofiber (Isogai, *et al*., 2011) (TOCNF, Nippon Paper Industries Co., Ltd., Japan) with a carboxylate content of 1.6 mM was stirred at 1500 rpm for 48 h before

use. The stirring process changed the TOCNF morphology from gel-like to a transparent liquid, whereas the bamboo-derived cellulose nanofiber prepared by the aqueous counter collision method (Kondo, *et al*., 2014) (ACC-CNF, Chuetsu Pulp & Paper Co., Ltd., Japan) was used as received. The dried cellulose membrane matrix was immersed in ACC-CNF and TOCNF dispersions. In this process, two independent variables were examined. First was the concentration of CNF dispersions for cellulose sponge immersion, which was set to 0.25%, 0.5%, 0.75%, and 1% mass percentage for one-time immersion. The other variable was the number of times that the sponge was immersed in 1% CNF solutions and was set to 1, 2, 4, and 7. The duration was 30 min for each immersion. The resulting composite sponges were dried at 65°C for 12 h to obtain TCNF- and MCNF-membranes. CNF sheets were fabricated by drying 10 g of CNF dispersion at 65°C for 24 h. A sheet of regenerated cellulose (RC) was fabricated by drying 15 g of xanthate solution at 65°C for 6 h and was then washed with warm water several times until the sheet became transparent.

1.3 Characterization of membrane

Electrophoresis and Dynamic Light Scattering (DLS) (Zetasizer Nano ZS, Malvern Instruments, UK) were applied to measure the zeta potential of a CNF dispersion and the oil droplet size of filtrates of TCNF membrane with TOCNF 15.8% deposited, and MCNF membrane with ACC-CNF 23.2% deposited. X-ray diffraction (XRD) was conducted to determine cellulose crystalline morphology using an X-ray diffractometer (D8 ADVANCE/TSM, Bruker Corporation, USA) with Cu-Kα as the radiation source at $\lambda = 1.5418$ Å. XPS analysis was carried out using a photoemission spectrometer (JPS-9010TR, JEOL, Japan). A xanthate sheet sample was prepared by drying a xanthate in a petri dish.

The microscopic structure of membranes was observed by scanning electron microscopy (SEM) (SU8020, Hitachi High-Technologies Corporation, Japan). Membrane photographs were obtained with a digital camera for macroscopic observation. Underwater contact angles of an oil droplet on membrane surfaces were measured by the sessile drop method (DropMaster DMs-401, Kyowa Interface Science Co., LTD., Japan) using canola oil (commercial grade, Trial Company Inc., Japan).

To evaluate feasibility, the separation efficiency and flowrate of the oil-water mixture were examined. As living sewage models, homogenous oil-water mixture and emulsion were prepared by mixing 5 mL of canola oil stained with Sudan blue II (Sigma-Aldrich, USA), 5 mL of distilled water, and with and without sodium dodecyl sulfate (Wako Pure Chemical Industries Ltd., Japan) as a surfactant. Subsequently, the mixture was stirred for at least 1 h at

800 rpm with a magnetic stirrer. The oil-water mixture and emulsion were poured into a filtration system immediately after stirring. The mass flowrate was determined by measuring the increasing mass of a filtrate over time. To measure the separation efficiency, a few mL sample taken from the final filtrate after shaking enough for homogeneity was dried at 65°C to evaporate the water for approximately 12 h until the mass did not change further. The remaining oil was then weighed. Separation efficiency was defined to be mass of water before and after separation (Cai, *et al*., 2017; Wen, *et al*., 2018) calculated using Equation. 5.1.

$$\text{Separation Efficiency } (\%) = \left(1 - \frac{C_l}{C_0}\right) \times 100\%, \tag{5.1}$$

where C_0 and C_l are the mass ratio of oil to oil-water mixture before and after separation, respectively.

5.3 Results and Discussion

5.3.1 Cellulose sponge and membrane fabrication

The mercerization process changes the cellulose crystal structure from native cellulose to mercerized cellulose that reacts with CS_2 to form water-soluble cellulose-CS_2Na (Fig. 5.1a). The XPS spectra shows peaks of C-C, C-O and O-C-O at 284.7, 286.2 and 287.6 eV of binding energy for filter paper cellulose as well as xanthate sheet. For the xanthate sheet, the C-C peak overlaps with the C-S peak at approximately 284.7 eV in binding energy (Fig. 5.1b) (Moulder, *et al*., 1992). In the regenerated cellulose, the bonding between cellulose and CS_2 was broken during dissolution of Na_3PO_4 with warm water. However, the xanthate sheet was washed with water only for detaching the sample from the petri dish; therefore, this washing process was not long enough to remove all residual CS_2 in the sheet. Fig. 5.1c shows the XRD patterns of filter paper, RC, ACC-CNF, and TOCNF. Filter paper has peaks at 14.5°, 16.5°, and 22.5° in 2θ corresponding to the $(1\bar{1}0)$, (110), and (200) planes, respectively, whereas RC has peaks at 12°, 20°, and 22° in 2θ corresponding to the $(1\bar{1}0)$, (110), and (020) planes, respectively (Nam, *et al*., 2016). TOCNF and ACC-CNF have the same peaks as filter paper. However, the 2θ peak of 16.5° disappears for TOCNF whereas the 2θ peak of 14.5° disappears for ACC-CNF. The 2θ peaks of 14.5° and 16.5° for filter paper and those of 12° and 20° for RC refer to the crystal configuration of cellulose rings and hydroxyl groups. Cellulose chains have hydrophobic sites located in the C-H bond of a glucose unit ring and hydrophilic sites located in three hydroxyl groups. This hydrophilic moiety can be arranged to (110) and $(1\bar{1}0)$ planes of a crystal lattice. The (110) plane does not have hydrogen bonds at the surface whereas the $(1\bar{1}0)$ plane only has hydrogen bonds at the surface (Yamane, *et al*., 2006; Isobe, *et al*., 2014).

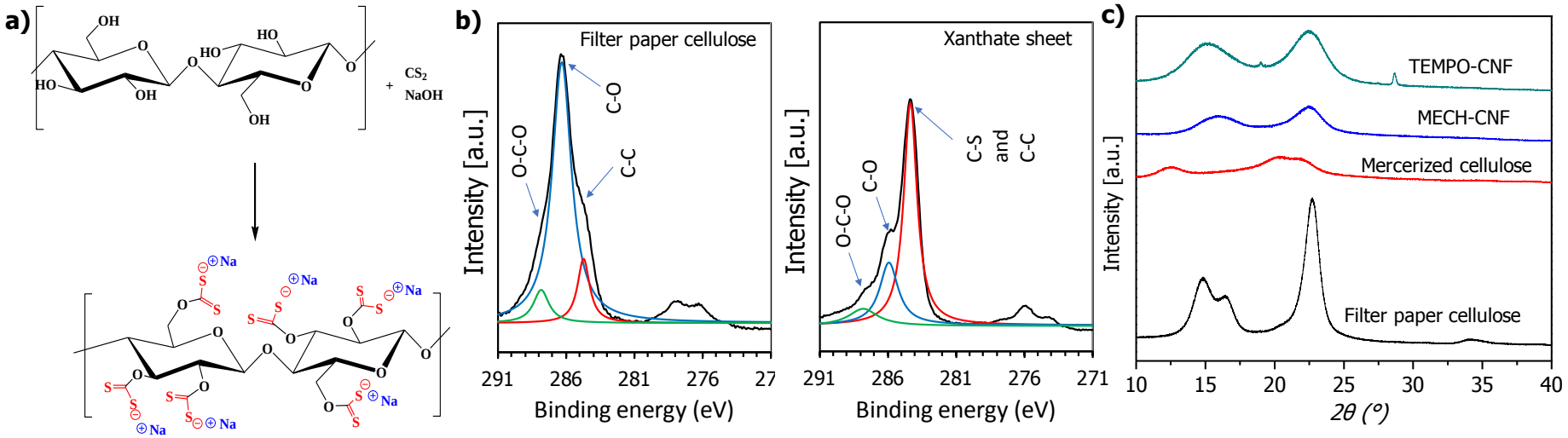

Fig. 5.1 Dissolution mechanisms of cellulose by xanthation (a), XPS spectra of filter paper cellulose and xanthate sheet (b), and XRD patterns of cellulose samples (c).

Fig. 5.4b shows the underwater OCA on CNF-membranes. A larger amount of CNF deposit significantly increased the OCA because the nanostructure of CNF exposed more hydroxyl groups and increased the roughness of the surface. The MCNF-membrane shows lower OCA than the TCNF-membrane. Besides the polar repulsion of water to hydrophobic oil molecules, electric repulsion also has a strong effect (Cheng, *et al*., 2017). TOCNF has carboxylic functional groups in cellulose molecular chains due to TEMPO oxidation (Zhao, *et al*., 2017). Therefore, TOCNF has a higher negative charge than the ACC-CNF according to the zeta potential measurement of TOCNF (-67.6 mV) and ACC-CNF (-33.5 mV) as mentioned in Chapter 3 (Fig. 3.7). In underwater conditions, impurities such as fatty acids contained in a hydrophobic liquid cause the surface of a droplet to be negatively charged (Roger & Cabane, 2012). Because a commercial grade of canola oil was applied, some fatty acids might be contained in the oil. A negatively charged droplet with a negatively charged surface would result in electric repulsion that provides TOCNF with higher underwater OCA compared ACC-CNF. Carboxylic groups-containing TOCNF are larger in molecular size than those in ACC-CNF, causing TOCNF to absorb and hold water easily so that it has a mucus-like structure and property, that is, a tendency to swell upon wetting as shown in Fig. 5.4a-*vii*.

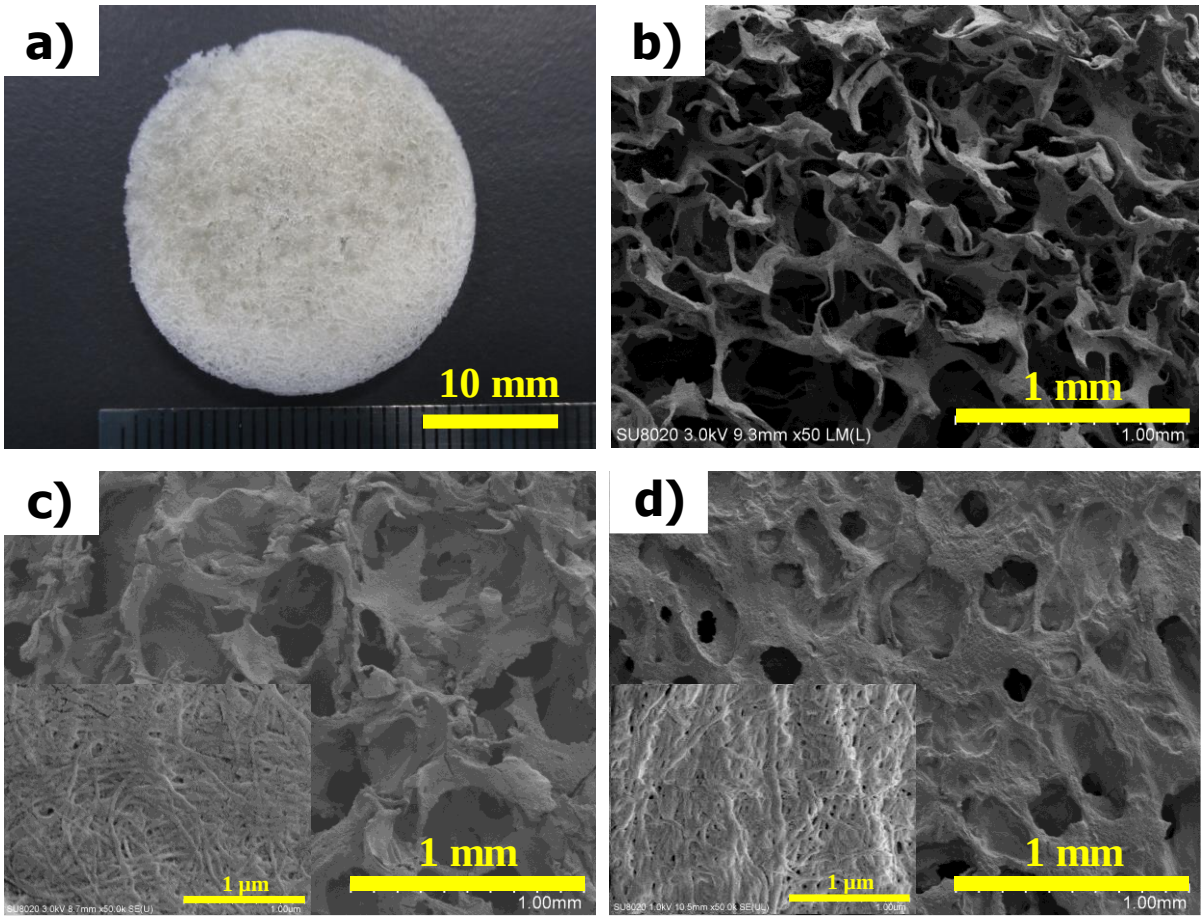

Fig. 5.2 Photograph of cellulose sponge (a), SEM images of cellulose sponge before CNF deposition (b), MCNF- (c) and TCNF- (d) membranes prepared by one-time immersion in 1% solutions with inserts at a high magnification.

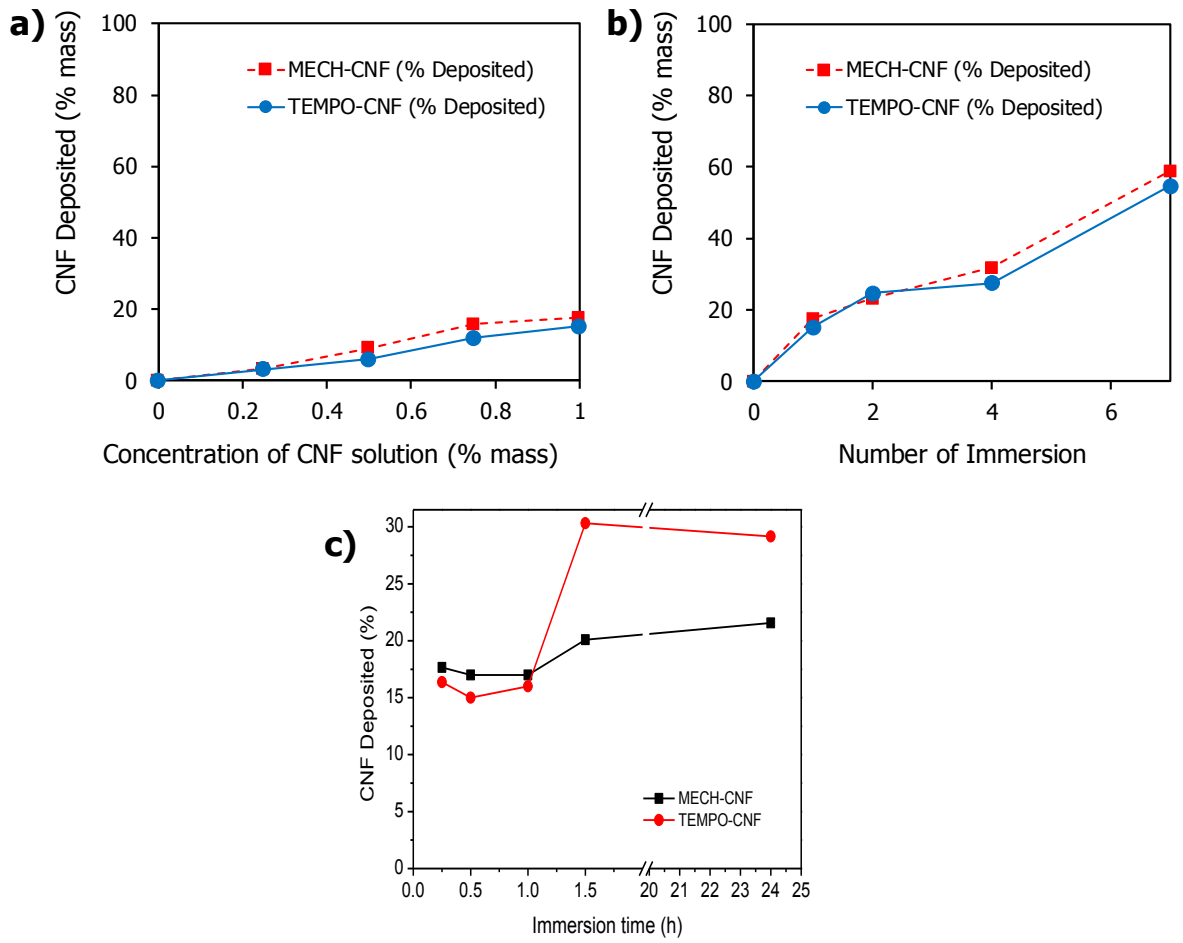

Fig. 5.3 Amount of MECH- and TOCNF deposited in the cellulose sponge depending on concentration (a) and number of immersions (b)

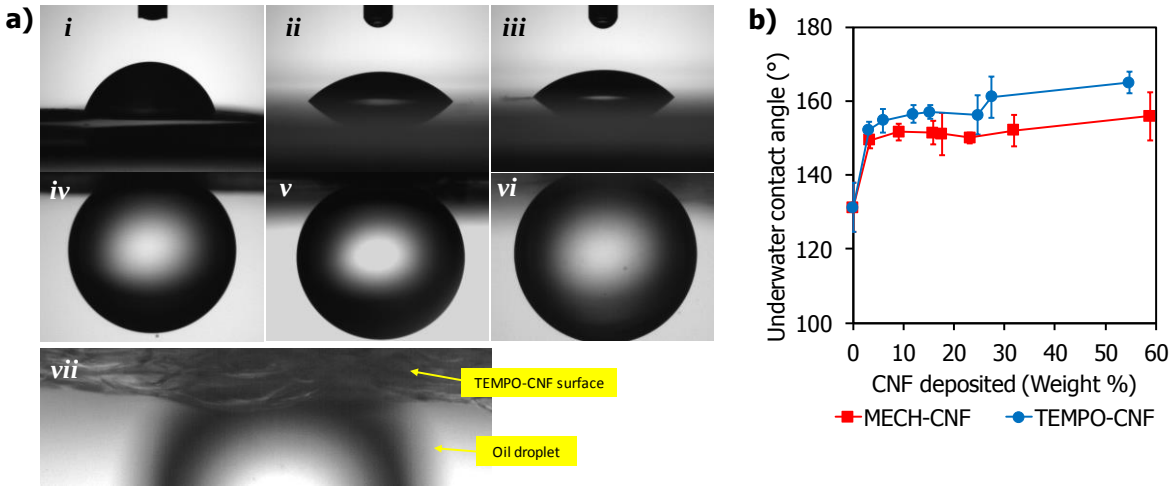

Fig. 5.4 In-air OCA on RC (a-i), ACC-CNF (a-ii), and TOCNF (a-iii) sheets and underwater OCA on RC (a-iv), ACC-CNF (a-v), and TOCNF (a-vi) sheets with magnified underwater interface between oil droplet and TOCNF sheet (a-vii), underwater contact angle of canola oil on cellulose membrane with CNF deposited in different amounts (b), and comparison in zeta potential between TOCNF and ACC-CNF dispersions (c).

5.4 Separation performance of cellulose membranes

The large OCA of the CNF-membrane has a potential application for oil-water separation. In the filtration tube, oil and water were separated slowly due to density differences. No oil attached to the membrane surface indicated that the surface has self-cleaning ability. The flowrate of the filtrate was affected by CNF deposition in the cellulose membranes as shown in Fig. 5.5a. With an increase in the CNF content, the flowrate was decreased. No penetration was observed for the MCNF-membrane upon immersion seven times and for the TCNF-membrane by only once immersion into a 1% CNF dispersion. All filtration processes were driven only by gravitational force. The flowrate when the MCNF- and TCNF-membranes were used for separation efficiency exceeding 98% were 3.73×10^3 and 166 L m^{-2} h^{-1}, respectively (Fig. 5.5b). This separation performance was better than that for previously reported membranes such as guar gum coated-stainless steel mesh (2850 L m^{-2} h^{-1}) (Wang, *et al*., 2017a) and graphene oxide@electrospun CNF (960 L m^{-2} h^{-1}) (Ao, *et al*., 2017). Even after using those membranes ten times repetitively, the high separation efficiency was maintained successfully (Fig. 5.5c). The flowrate of TCNF-membranes decreased significantly after using ten times due to high water absorption (Fig. 5.5d). However, the membrane failed to separate oil-water emulsion. All of the oil passed through the membrane.

Separation and flowrate depend on different mechanisms. For separation, pore diameters of the membrane are required to be are only slightly lower smaller than the diameter of oil droplet diameter is necessary (Schutzius, *et al*., 2017). However, for the flowrate, the rate depends on the pressure and pore size diameter. Smaller pore size will decrease the flowrate. Darcy's law for flowrate at porous material are given by in (Cummins, *et al*., 2017):

$$Q = \frac{\kappa A \Delta P}{\mu L} \tag{5.2}$$

where, Q is the volumetric flow rate, A is the cross-sectional area of all porous, and ΔP is the pressure drop, μ is viscosity, κ is the permeability and a measurement of how easily fluid can flow through a given porous material, shows that the flowrate decreases simultaneously by decreasing the pore size. As shown in Fig. 5.5a, the flowrate of TCNF-membranes decreased more significantly compare to MCNF-membranes because the pore size of TCNF-membranes significantly decreased due to high water absorption. However, as the pore size of membranes reach slightly lower than droplet size, the oil droplet was rejected and the separation efficiency increased significantly as shown in Fig. 5.5b.

TOCNF contains many carboxylic groups that absorb water forming a more gel-like appearance compared to ACC-CNF. This gelling property blocked the membrane pores and decreased the flux of water. External pressure is an important factor to increase the flux. As the external pressure induced by gravity was lower than the breakthrough pressure, the membrane rejected the percolation of oil (Dai, *et al*., 2017). The oil-water separation condition is schematically depicted in Fig. 5.6.

Breakthrough pressure is defined as Equation. 2.12 (Xue, *et al*., 2011; Chen, *et al*., 2013)

$$P_{\text{breakthrough}} = -\frac{2\gamma_{OW}\cos\theta}{d}, \tag{2.12}$$

where $P_{\text{breakthrough}}$, γ_{OW}, d, and θ are the breakthrough pressure, interfacial surface tension between oil and water, diameter of a pore, and OCA against water, respectively. The γ_{OW} of canola oil is 0.031 N/m (Gaonkar, 1989), an underwater OCA θ can be measured, and P is equivalent to gravitational pressure $P_g = \rho g h$ if the external pressure is limited to gravity, where ρ is the density of canola oil (906 kg/m^3), g is the gravitational acceleration (9.81 m/s^2), and h is the height of the oil-water mixture in the filter holder during the experiment (0.045 m). By these substitutions the maximum limit value of d is calculated to be approximately 129 μm. Higher values than this limit will let the oil droplet pass through the membrane whereas smaller values of d will detain oil droplets. However, the maximum pore size of the membrane that repels oil while maintaining the high flowrate is slightly smaller than the oil droplet diameter (Xue, *et al*., 2011; Tian, *et al*., 2012; Schutzius, *et al*., 2017). The separation process of oil-water mixture is shown in Fig. 5.7a.

Immediately after stirring the mixture still contains small oil drops. Higher porosity will increase the flux but decrease the separation efficiency as implied by Equation. 2.12. Namely, during the separation process, small droplets contact the membrane surface and are then repelled; these droplets will coagulate and due to a lower density than water, the oil will migrate to near the water level. However, if small oil droplets are not rejected because of low surface oleophilicity corresponding to low underwater OCA or a large enough pore size (large d), these droplets will penetrate the membrane, thus causing poor rejection. After separation, the small oil droplets did not penetrate the membrane for more than 2 hours as shown in Fig. 5.7b. The DLS measurement shows that the particulates had diameter of 619 and 678 nm for filtrate of MCNF membrane and TCNF membrane, respectively. The separation efficiency did not change significantly during repeated separation processes. This result indicates that the

membrane surface repelled oil and only allowed water to pass through the membrane without causing any serious damage to the filter materials. After several times of separation, TCNF-membranes flowrate declined due to decreasing porosity by water absorption.

For comparison, other polysaccharide-based membranes reported in the past are listed in Table 5.1. The MCNF membrane in this work shows comparable separation efficiency and flowrate. In addition, this membrane system needs no pressurizing system as a driving force except gravity and provides self-cleaning ability because of the oleophobic surface sourced from ACC-CNF.

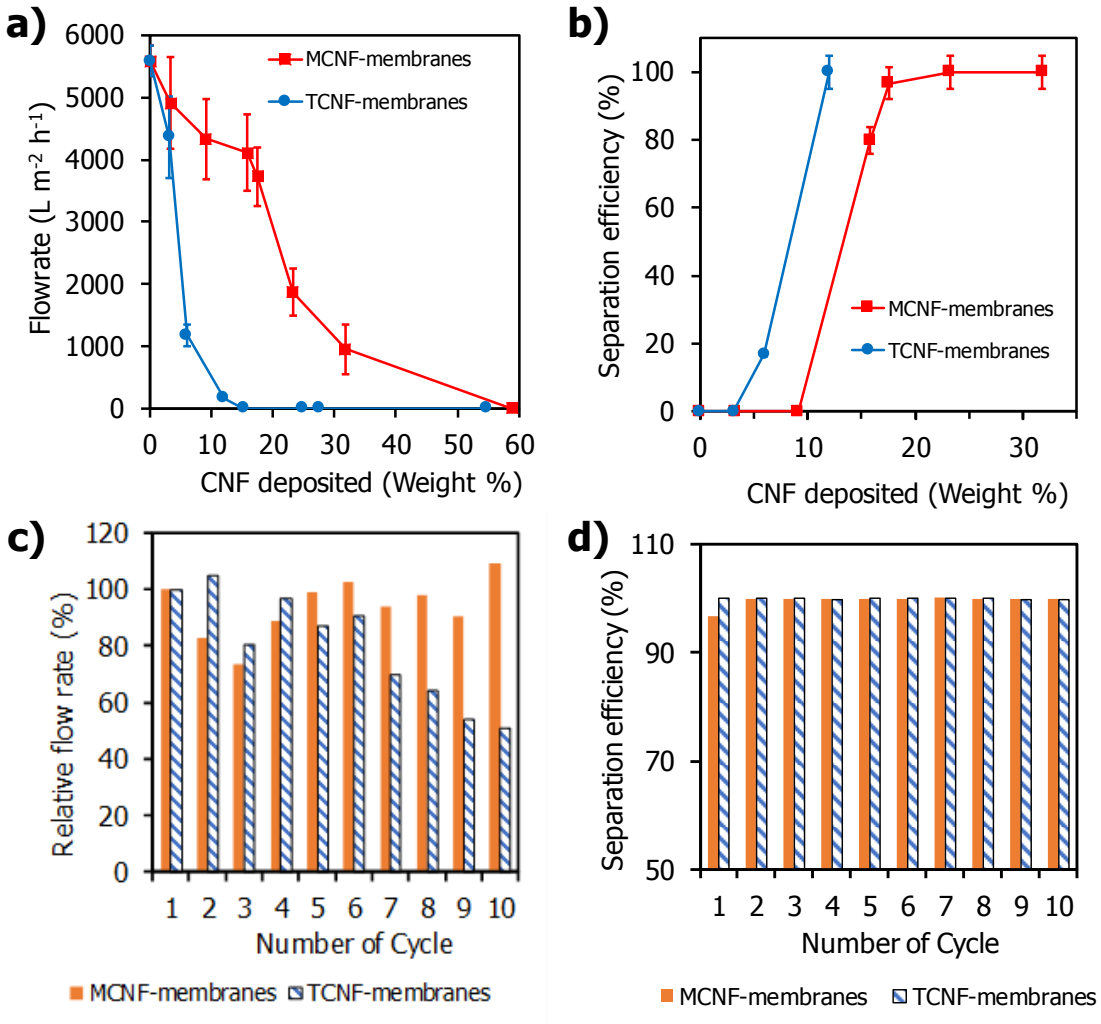

Fig. 5.5 Flowrate (a) and separation efficiency (b) of MCNF- and TCNF-membranes, flowrate (c) and separation efficiency (d) of 17.55% deposited MCNF and 11.97% deposited TCNF after several times cycle.

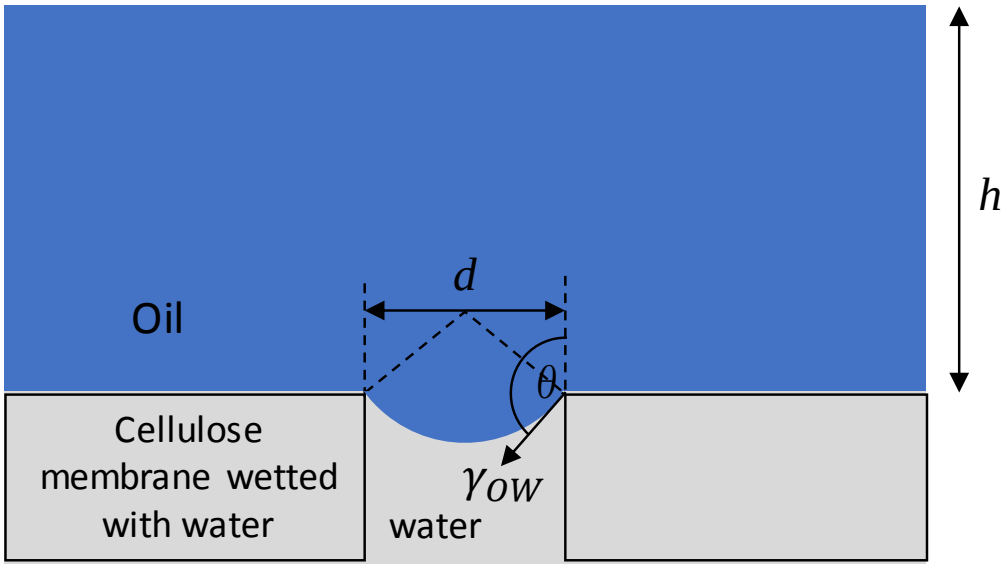

Fig. 5.6 Schematic diagram of the oil-water separation mechanism.

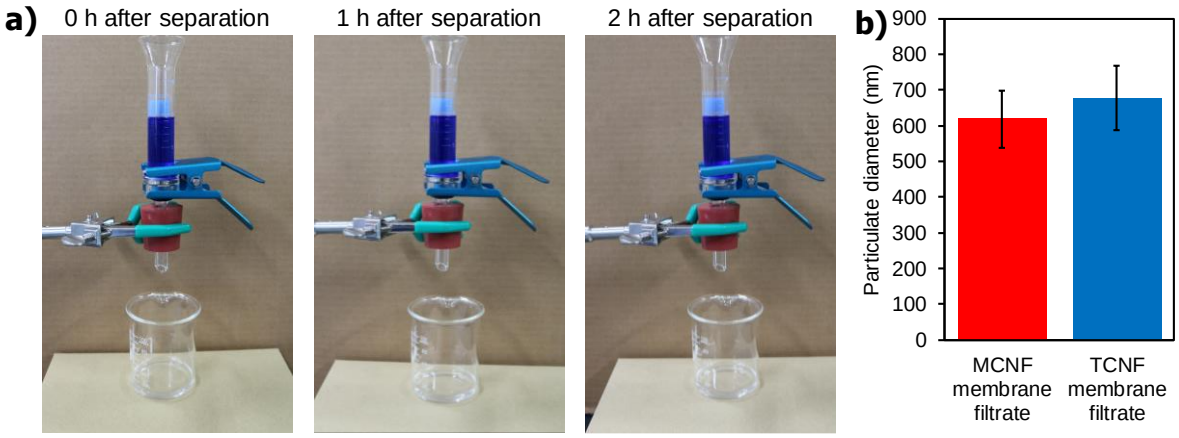

Fig. 5.7 (a) Photographs of the filtration system after filtering process was completed using MCNF membrane with ACC-CNF deposited at 23.2%) and (b) particulate diameter of filtrates from MCNF membrane with ACC-CNF deposited at 23.2% and TCNF membrane with TOCNF deposited at 15.8%.

Table 5.1 Comparison of CNF-deposited cellulose membrane to other base materials

Material	Type of Oil	Wettability	Flowrate	Separation Efficiency	Force	Ref
MCNF-deposited cellulose sponge	Canola oil	Underwater superoleophobic	3.73×10^3 L m^{-2} h^{-1}	98.5%	gravity	This work
TCNF-deposited cellulose sponge	Canola oil	Underwater superoleophobic	166 L m^{-2} h^{-1}	99.98%	gravity	This work
Filter paper coated with polystyrene grain, polyethylene terephthalate, silica	Diesel oil	Superoleophilic, superhydrophobic	Data unavailable	>96%	gravity	Wang, *et al*., 2010
Cellulose sponge coated with Fe_3PO_4 and hexadecyl trimethoxy silane	Toluene	Superoleophilic	350 kg m^{-2} h^{-1} bar^{-1}	95%	vacuum	Peng, *et al*., 2016
Melamine sponge coated with chitosan-Sodium perfluorononanoate and Fe_3PO_4	Soybean oil	Superhydrophilic, superoleophobic	Data unavailable	96%	gravity	Su, *et al*., 2017
PVDF membrane coated with chitosan silica	Gasoline emulsion	Underwater superoleophobic (emulsion)	Data unavailable	>99%	vacuum	Liu, *et al*., 2016
polyvinylidene fluoride-co-hexafluoropropylene (PVDF–HFP) nanofibers modified with cellulose	Corn oil	Superhydrophilic and underwater superoleophobic	250 L m^{-2} h^{-1} bar^{-1}	>99.98%	vacuum	Ahmed, *et al*., 2014
Polyvinyl alcohol coated filter paper	Petroleum based oil	Superhydrophilic and underwater superoleophobic	Data unavailable	>99%	gravity	Fan, *et al*., 2015
TOCNF coated filter paper	n-hexane emulsion	underwater superoleophobic	89.6 L m^{-2} h^{-1}	>99%	gravity	Rohrbach, *et al*., 2014
Cellulose sponge freeze drying	Toluene emulsion	underwater superoleophobic	91 L m^{-2} h^{-1}	>99.94%	gravity	Wang, *et al*., 2015b

Cellulose coated nylon mesh	Petroleum based oil	underwater superoleophobic	Data unavailable	>99.99%	gravity	Lu, *et al*., 2014
Cellulose nanosheet-supported cellulose acetate	Ferritin	Underwater superoleophobic	1620 L m^{-2} h^{-1} bar^{-1}	92.5%	vacuum	Zhou, *et al*., 2014
Tunicate cellulose nanocrystal coated nylon membrane	n-hexane emulsion	Underwater superoleophobicity	1549 L m^{-2} h^{-1} bar^{-1}	99.99%	vacuum	Cheng, *et al*., 2017
Alginate graphene oxide	Kerosene	Underwater superoleophobic	13680 L m^{-2} h^{-1}	99.6%	gravity	Li, *et al*., 2017
Polyvinylpyrrolidone modified cotton	n-hexane	Underwater superoleophobic	66800 L m^{-2} h^{-1}	Data unavailable	gravity	Wang, *et al*., 2017b
Freeze drying CNF chitosan	Soybean oil	Underwater oleophobic	13680 L m^{-2} h^{-1}	Data unavailable	gravity	Wang, *et al*., 2017a
Graphene oxide@electrospun CNF	n-hexane	Underwater superoleophobic	2850 L m^{-2} h^{-1}	99.6%	gravity	Ao, *et al*., 2017
Guar gum coated stainless steel mesh	cyclohexane	Superoleophobic	960 L m^{-2} h^{-1}	>99%	gravity	Dai, *et al*., 2017

5.4 Conclusion

A cellulose sponge with sufficient mechanical strength was fabricated successfully. Deposition of TCNF and bamboo-sourced MCNF on the inner pore surfaces of the sponge showed underwater superoleophobic and in-air oleophilic properties. The TCNF deposit behaved as a mucus-like layer when immersed in water and enhanced oil repellency and provided separation efficiency greater than the MCNF deposit. However, the mucus-like layer absorbed much water and decreased the flowrate. Oil-water separation testing demonstrated an excellent separation efficiency (>99% and >98% for MCNF- and TCNF-membranes, respectively) and a high flowrate (3.73×10^3 and 166 L m^{-2} h^{-1} for MCNF- and TCNF membranes, respectively) with gravitational force alone.

References

Ahmed, F. E., Lalia, B. S., Hilal, N., & Hashaikeh, R. (2014). Underwater Superoleophobic Cellulose/Electrospun PVDF-HFP Membranes for Efficient Oil/Water Separation. *Desalination*, 344, 48-54.

Ao, C., Yuan, W., Zhao, J., He, X., Zhang, X., Li, Q., Xia, T., Zhang, W., Lu, C. (2017). Superhydrophilic Graphene Oxide@Electrospun Cellulose Nanofiber Hybrid Membrane for High-Efficiency Oil/Water Separation. Carbohydrate Polymers, 175, 216-222.

Cai, Y., Chen, D., Li, N., Xu, Q., Li, H., He, J., and Lu, J. (2017). Nanofibrous metal-organic framework composite membrane for selective efficient oil/water emulsion separation. *Journal of Membrane Science*, 543, 10-17.

Chen, P.-C., & Xu, Z.-K. (2013). Mineral-Coated Polymer Membranes with Superhydrophylicity and Underwater Superoleophobicity for Effective Oil/Water Separation. *Scientific Reports*, 3, 2776.

Cheng, Q., Ye, D., Chang, C., & Zhang, L. (2017). Facile Fabrication of Superhydrophilic Membranes Consisted of Fibrous Tunicate Cellulose Nanocrystals for Highly Efficient Oil/Water Separation. *Journal of Membrane Science*, 525, 1-8.

Coelho, G., Clark, J., and Aurand, D. (2013). Toxicity testing of dispersed oil requires adherence to standardized protocols to assess potential real world effects. *Environmental Pollution*, 177, 185-188.

Committee on the Effects of the Deepwater Horizon Mississippi Canyon-252 Oil Spill on Ecosystem Services in the Gulf of Mexico, "Oil spill response technologies," in An ecosystem services approach to assessing the impacts of the deepwater horizon oil spill in the gulf of mexico , Washington DC, The National Academic Press, 2013, p. 71.

Cummins, B. M., Chinthapatla, R., Ligler, F. S., Walker, G. M. (2017). Time-Dependent Model for Fluid Flow in Porous Materials with Multiple Pore Sizes. *Analytical Chemistry*, 89(8), 4377-4381.

Dai, L., Wang, B., An, X., Zhang, L., Khan, A., & Ni, Y. (2017). Oil/Water Interfaces of Guar Gum-based Biopolymer Hydrogels and Application to Their Separation. Carbohydrate Polymers, 169, 9-15.

Fan, J.-B., Song, Y., Wang, S., Meng, J., Yang, G., Guo, X., Feng, L., Jiang, L. (2015). Directly Coating Hydrogel on Filter Paper for Effective Oil-Water Separation in Highly Acidic, Alkaline, and Salty Environment. *Advanced Functional Materials*, 25, 5368-5375.

Gaonkar, A. G. (1989). Interfacial Tensions of Vegetable Oil/Water Systems: Effect of Oil Purification. Journal of the American Oil Chemists' Society, 66(8), 1090-1092.

Huang, S. and Wang, D. (2017). A simple nanocellulose coating for self-cleaning upon water action: molecular design of stable surface hydrophilicity. *Angewandte Chemie International Edition*, 56, 9053-9057.

Isobe, N., Nishiyama, Y., Kimura, S., Wada, M., & Kuga, S. (2014). Origin of Hydrophilicity of Cellulose Hydrogel from Aqueous LiOH/Urea Solvent Coagulated with Alkyl Alcohols. Cellulose, 21, 1043-1050.

Isogai, A., Saito, T., Fukuzumi, H.(2011). TEMPO-oxidized cellulose nanofibers. *Nanoscale*, 3, 71-85.

Kondo, T., Kose, R., Naito, H., & Kasai, W. (2014). Aqueous counter collision using paired water jets as a novel means of preparing bio-nanofibers. Carbohydrate Polymers, 112, 284-290.

Li, Y., Zhang, H., Fan, M., Zheng, P., Zhuang, J., & Chen, L. (2017). A Robust Salt-Tolerant Superoleophobic Alginate/Graphene Oxide Aerogel for Efficient Oil/Water Separation in Marine Environments. *Scientific Reports*, 7, 46379.

Liu, J., Li, P., Chen, L., Feng, Y., He, W., & Lv, X. (2016). Modified Superhydrophilic and Underwater Superoleophobic PVDF Membrane with Ultralow Oil-Adhesion for Highly Efficient Oil/Water Emulsion Separation. *Materials Letters*, 185, 169-172.

Lu, F., Chen, Y., Liu, N., Cao, Y., Xu, L., Wei, Y., & Feng, L. (2014). A Fast and Convenient Cellulose Hydrogel-Coated Colander for High-Efficiency Oil-Water Separation. *RSC Advances*, 4, 32544-32548.

Moberg, T., Sahlin, K., Yao, K., Geng, S., Westman, G., Zhou, Q., Oksman, K., Rigdahl, M. (2017). Rheological properties of nanocellulose suspensions: effects of fibril/particle dimensions and surface characteristics. Cellulose, 24(6), 2499-2510.

Moulder, J. F., Stickle, W. F., Sobol, P. E., Bomben, K. D. (1992). *Handbook of X-ray photoelectron spectroscopy*. J. Chastain, Ed., Eden Prairie, Minnesota: Perkin-Elmer Corporation.

Nam, S., French, A. D., Condon, B. D., & Concha, M. (2016). Segal crystallinity index revisited by the simulation of X-ray diffraction patterns of cotton cellulose Iβ and cellulose II. Carbohydrate Polymers, 135, 1-9.

Nasution, M. A., Wibawa, D. S., Ahamed, T. and Noguchi, R. (2018). Comparative environmental impact evaluation of palm oil mill effluent treatment using a life cycle assessment approach: A case study based on composting and a combination for biogas

technologies in North Sumatera of Indonesia. *Journal of Cleaner Production*, 184, 1028-1040.

Nechyporchuk, O., Belgacem, M. N., & Pignon, F. (2016). Current Progress in Rheology of Cellulose Nanofibril Suspensions. Biomacromolecules, 17(7), 2311-2320.

Obaid, M., Yang, E., Kang, D.-H., Yoon, M.-H., Kim, I. S. (2018). Underwater superoleophobic modified polysulfone electrospun membrane with efficient antifouling for ultrafast gravitational oil-water separation. *Separation and Purification Technology*, 200, 284-293.

Padaki, M., Murali, R. S., Abdullah, M. S., Misdan, N., Moslehyani, A., Kassim, M. A., Hilal, N., Ismail, A. F. (2015) Membrane technology enhancement in oil-water separation. A review. *Desalination*, 357, 197-207.

Pi, P., Hou, K., Zhou, C., Wen, X., Xu, S., Cheng, J. (2016). A novel superhydrophilic-underwater superoleophobic Cu2S coated copper mesh for efficient oil-water separation. *Materials Letters*, 182, 68-71.

Roger, K., & Cabane, B. (2012). Why Are Hydrophobic/Water Interfaces Negatively Charged? *Angewandte Chemie, 124*, 5723-5726.

Rohrbach, K., Li, Y., Zhu, H., Liu, Z., Dai, J., Andreasen, J., & Hu, L. (2014). A cellulose based hydrophilic, oleophobic hydrated filter for water/oil separation. *Chemical Communications*, 50, 13296-13299.

Schutzius, T. M., Walker, C., Maitra, T., Schonherr, R., Stamatopoulos, C., Jung, S., Antonini, C., Eghlidi, H., Fife, J. L., Patera, A., Derome, D., Poulikakos, D. (2017). Detergency and Its Implications for Oil Emulsion Sieving and Separation. *Langmuir*, 33, 4250-4259.

Song, J., Huang, S., Lu, Y., Bu, X., Mates, J. E., Ghosh, A., Ganguly, R., Carmalt, C. J., Parkin, I. P., Xu, W. and Megaridis, C. M. (2014). Self-driven one-step oil removal from oil spill on water via selective-wettability steel mesh. *ACS Applied Materials & Interfaces*, 6, 19858-19865.

Su, C., Yang, H., Song, S., Lu, B., & Chen, R. (2017). A Magnetic Superhydrophilic/Oleophobic Sponge for Continuous Oil-Water Separation. *Chemical Engineering Journal*, 309, 366-373.

Tian, D., Zhang, X., Tian, Y., Wu, Y., Wang, X., Zhai, J., and Jiang, L. (2012). Photo-induced water-oil separation based on switchable superhydrophobicity-superhydrophilicity and underwater superoleophobicity of the aligned ZnO nanorod array-coated mesh films, *Journal of Materials Chemistry*, 22, 19652-19657.

Tuteja, A., Choi, W., Ma, M., Mabry, J. M., Mazzella, S. A., Rutledge, G. C., McKinley, G. H. and Cohen, R. E. (2007). Designing superoleophobic surfaces. *Science*, 318, 1618-1622.

Wang, C.-F., Huang, H.-C., & Chen, L.-T. (2015a). Protonated Melamine Sponge for Effective Oil/Water Separation. *Scientific Reports*, 5, 14294.

Wang, G., He, Y., Wang, H., Zhang, L., Yu, Q., Peng, S., Wu, X., Ren, T., Zeng, Z., Xue, Q. (2015b). A Cellulose Sponge with Robust Superhydrophilicity and Under-water Superoleophobicity for Highly Effective Oil/Water Separation. *Green Chemistry*, 17, 3093-3099.

Wang, Y., Uetani, K., Liu, S., Zhang, X., Wang, Y., Lu, P., Wei, T., Fan, Z., Shen, J., Yu, H., Li, S., Zhang, Q., Li, Q., Fan, J., Yang, N., Wang, Q., Liu, Y., Cao, J., Li, J., Chen, W. (2017a). Multi-functional Bionanocomposite Foams Using a Chitosan. ChemNanoMat, 3(2), 98-108

Wang, C.-F., Yang, S.-Y., & Kuo, S.-W. (2017b). Eco-Friendly Superwetting Material for Highly Effective Separations of Oil/Water Mixtures and Oil-in-Water Emulsions. *Scientific Reports*, 7, 43053. doi: 10.1038/srep43053

Wang, Z., Elimelech, M. and Lin, S. (2016). Environmental applications of interfacial materials with special wettability. *Environmental Science and Technology*, 50, 2132-2150.

Wen, N., Miao, X., Yang, X., Long, M., Deng, W., Zhou, Q., Deng, W. (2018). An alternative fabrication of underoil superhydrophobic or underwater superoleophobic stainless steel meshes for oil-water separation: Originating from one-step vapor deposition of polydimethylsiloxane. *Separation and Purification Technology*, 204, 116-126.

Xue, Z., Wang, S., Lin, L., Chen, L., Liu, M., Feng, L., and Jiang, L. (2011). A novel superhydrophilic and underwater superoleophobic hydrogel-coated mesh for oil/water separation. *Advanced Materials*, 23, 4270-4273.

Yamane, C., Aoyagi, T., Ago, M., & Sato, K. (2006). Two Different Surface Properties of Regenerated Cellulose due to Structural Anisotropy. Polymer Journal, 38(8), 819-826.

Yang, H.-C., Hou, J., Chen, V., Xu. Z.-K. (2016). Janus membranes: exploring duality for advanced separation. *Angewandte Chemie International Edition*, 55(43), 13398-13407.

Yang, J., Yin, L., Tang, H., Song, H., Gao, X., Liang, K., & Li, C. (2015). Polyelectrolyte-fluorosurfactant Complex-based Meshes with Superhydrophilicity and

Superoleophobicity for Oil/Water Separation. *Chemical Engineering Journal*, 268, 245-250.

Ye, S., Cao, Q., Wang, Q., Wang, T., and Peng, Q. 2016. A highly efficient, stable, durable, and recyclable filter fabricated by femtosecond laser drilling of a titanium foil for oil-water separation. *Scientific Reports*, 6, 37591, doi: 10.1038/srep37591

Yue, X., Zhang, T., Yang, D., Qiu, F., Li, Z. (2018). Ultralong MnO2 nanowire enhanced multiwall carbon nanotube hybrid membrane with underwater superoleophobicity for efficient oil-in-water emulsions separation. *Industrial & Engineering Chemistry Research*, 57(31), 10439-10447.

Zeiger, C., Kumberg, J., Vullers, F., Worgull, M., Holscher, H., and Kavalenka, M. N. (2017). Selective filtration of oil/water mixtures with bioinspired porous membranes. *RSC Advances*, 7, 32806-32811.

Zhang, F., Gao, S., Zhu, Y., Jin, J. (2016). Alkaline-induced superhydrophilic/underwater superoleophobic polyacrylonitrile membranes with ultralow oil-adhesion for high-efficient oil/water separation. *Journal of Membrane Science*, 513, 67-73.

Zhang, W., Zhu, Y., Liu, X., Wang, D., Li, J., Jiang, L., Jin, J. (2014). Salt-induced fabrication of superhydrophilic and underwater superoleophobic PAA-g-PVDF membranes for effective separation of oil-in-water emulsions. *Angewandte Chemie International Edition*, 53, 856-860.

Zhao, Y., Moser, C., Lindstrom, M. E., Henriksson, G., & Li, J. (2017). Cellulose Nanofibers from Softwood, Hardwood, and Tunicate: Preparation-Structure-Film Performance Interrelation. ACS Applied Materials & Interfaces, 9, 13508-13519.

Zhou, K., Zhang, Q. G., Li, H. M., Guo, N. N., Zhu, A. M., & Liu, Q. L. (2014). Ultrathin Cellulose Nanosheet Membranes for Superfast Separation of Oil-in-Water Nanoemulsions. *Nanoscale*, 6, 10363-10369.

Chapter 6 Overall Conclusion

Under several concentration of ethanol water solution, the cellulose nanofiber exhibited superoleophobic properties. The experimental and calculated contact angle showed a high deviation for high ethanol concentration and low deviation for low ethanol concentration. The difference due to surface change properties including absorption, zeta potential and roughness of cellulose nanofiber under solution environment. TOCNF surface also showed a mucus fish scale like surface. Antifouling experiment reveal that CNF capable to repel oil and has antifouling properties.

For supporting materials, cellulose sponge was fabricated through xanthation method for cellulose dissolution followed by drying for regeneration. The drying was consist of two steps; first steps affected by mass and heat transfer due to mass and temperature difference between sample and environment followed by convective mass transfer in second step after the sample temperature reach as environment temperature. The values of activation energy and pre-exponential factor during convective mass transfer were -20.5 kJ K^{-1} mol^{-1} and 2250 m^{-2} s^{-1}, respectively. No tendency between the physical strength of obtained cellulose sponge and drying temperature. Addition of CNF to the xanthate did not affect the physical strength of obtained cellulose sponge. However, sponge obtained from 65 ˚C of drying temperature showed more stable physical strength.

The fabrication of cellulose sponge coated with CNF was fabricated successfully. Cellulose sponge with relatively high physical strength act as supporting material, while CNF act as active superoleophobic material. Deposition of TOCNF and ACC-CNF on the inner pore surfaces of the sponge showed underwater superoleophobic and in-air oleophilic properties. Mucus-like layer of TOCNF enhanced oil repellency and provided separation efficiency greater than the ACC-CNF deposit. However, the mucus-like layer absorbed much water and decreased the flowrate. Oil-water separation testing demonstrated an excellent separation efficiency (>99% and >98% for MCNF- and TCNF-membranes, respectively) and a high flowrate (3.73×10^3 and 166 L m^{-2} h^{-1} for MCNF- and TCNF membranes, respectively) with gravitational force alone.